भारतीय प्रौद्योगिकी संस्थान गुवाहाटी
Indian Institute of Technology Guwahati

APPLICATION OF ELECTROMAGNETICS IN FORMING OF TUBES AND PERFORATION OF SHEETS

A Thesis Submitted in Partial Fulfilment of the Requirements for the Degree of

Doctor of Philosophy

by

Chandrahas Patel
(Roll No. 11610323)

Department of Mechanical Engineering
Indian Institute of Technology Guwahati
Guwahati : 781039, India

October 2017

C E R T I F I C A T E

It is certified that the work contained in the thesis titled "**Application of Electromagnetics in Forming of Tubes and Perforation of Sheets**" by **Chandrahas Patel** (Roll No. **11610323**) has been carried out under my supervision and this work has not been submitted elsewhere for a degree.

Date: 31/10/2017

Dr. Sachin D. Kore

Associate Professor

Indian Institute of Technology Guwahati

A C K N O W L E D G M E N T S

There are many people who have directly or indirectly contributed to my doctoral research work. Before presenting my research work, I would like to take the opportunity to humbly acknowledge all of them for their constant support and guidance.

First and foremost, I would like to thank my supervisor Dr. Sachin D. Kore for his guidance and intellectual inputs throughout the completion of the research work. He showed tremendous confidence in me and was very patient, for which I shall always be indebted to him. I appreciated all his contributions of time and ideas to make my doctoral research experience productive and stimulating. I thank the members of my doctoral committee: Prof. U. S. Dixit (Chairman), Dr. R. Ganesh Narayanan and Prof. P. Poulose for their time, encouragement and valuable suggestions during my doctoral research work. I am also grateful to former and present heads of the Department of Mechanical Engineering, Prof. Prof. A.K. Dass and Prof. S. K. Dwivedy for extending various facilities during the tenure of my doctoral program.

I wish to express my sincere thanks to Mr. Jiten Basumatary, Mr. Amal Kalita, Mr. Nip Borah and Mr. S. Ahmed for their assistance during the experimental work. I sincerely thank Mr. N. K. Das, Mr. D. Chetri, Mr. N. Saikia, Mr. M. Sarma, Mr. B. Chandan, Mr. U. Gohain and Mr. M.C. Medhi for their help in conducting experiments.

I express my sincere thanks to my friends Mr. Jyoti Doley, Mr. Ashish Rajak, Mr. Ramesh Kumar, Mr. Piyush Singh, Mr. Getu T. Areda, Mr. Sagar Pawar, Mr. Raushan Kumar for their help and encouragement. My sincere thanks to Mr. Praveen Ghatule, Mr. Ashutosh Sahoo, Mr. Bhupendra Dhakad and Mr. Deepak Patel for their help in experimental and simulation work. My sincere thanks also go to Dr. Ravikant, Dr. Vinod Yadav, Mr. Saptarshi Karmakar, Mr. Dhruv Kashyap, Dr. Vijay Mishra.

I will always be grateful to my parents (Mr. Balram Patel and Ms. Madhuri Patel), my brother Mr. Vinal Patel and my sister Ms. Isha Patel for their unconditional love, support and encouragement during my research work.

TABLE OF CONTENTS

LIST OF FIGURES

LIST OF TABLES

ABSTRACT

Electromagnetic forming (EMF) is a high strain rate forming process that utilizes high strength electromagnetic pressure to form tubes and sheets into the desired shape. High strain rate forming process successfully addresses the problems faced in conventional forming techniques. It can be effectively used for forming metals with low formability like aluminium alloys. It can be instrumental in the manufacturing of lighter vehicles with higher fuel efficiency.

Although electromagnetic forming has been known for decades, its industrial use has risen in recent years. Electromagnetic forming is a high-speed forming process and many simulations have been carried out to know the effect of various parameters during the process. In the present study, the emphasis is on the study of the electromagnetic forming of tubes and sheets with application to simultaneous electromagnetic forming and perforation of sheets.

In the case of electromagnetic tube expansion, the effect of various parameters during forming has been studied experimentally and numerically. The effect of coil-tube relative length has been studied by varying the coil length, to obtain different tube geometries as the coil length is changed. The electromagnetic tube expansion is simulated and validated with the experimental results. The validated model is used to study the effect of various parameters during electromagnetic tube expansion. As frequency is one of the important parameters during electromagnetic tube forming, the study on the effect of electromagnetic tube expansion has been carried out, and the optimum frequency range is found out based on the final deformation of the tube.

The input current used for the electromagnetic forming is of damped sinusoidal form, only first few pulses are contributing in metal forming while rest of the successive pulses are not significantly contributing towards forming. The effect of current pulse contribution during electromagnetic forming is studied by crowbarring the successive current pulses. The simulation result shows that only a part of the current pulse is responsible for forming. In the case of electromagnetic sheet forming, a spiral coil is used as an actuator that has a drawback of central dead zone leading to inefficient forming. Hence to increase the efficiency of the electromagnetic sheet forming, dual electromagnetic forming of the sheet using uniform pressure actuator has been proposed.

To carry out the simultaneous forming and perforation of the sheet, feasibility study of electromagnetic forming and perforation of the sheet has been carried out. By performing electromagnetic forming and perforation experiments of the sheet, optimum energy required to carry out the operation has been obtained. Finally, the minimum velocity required to perform the electromagnetic forming and perforation has been determined.

CHAPTER 1

Introduction

The increasing concern about global warming and increasing fuel efficiency of the vehicle has led manufacturers to look for innovative technologies. Lightweight design is one of the ways to reduce vehicle emission and increasing fuel efficiency. Some lightweight design approaches include vehicle downsizing and redesign, but they may lead to adverse effect on customer comfort and safety. Therefore, vehicle manufacturers are looking for advanced materials and technologies to incorporate lightweight design in their system. Aluminium is considered as an alternative to steel for vehicle body design, but one of the problems with application of aluminium is its lower formability due to low strain hardening exponent and strain rate sensitivity values. The high strain rate forming processes were found to increase the formability of aluminium. In the search for new technologies to improve the formability of aluminium, electromagnetic forming is considered in the present work. The present study is concerned with the study of electromagnetic forming and its application to the electromagnetic forming and perforation of sheets.

1.1 Metal Forming

The metal forming process is a type of manufacturing process in which metal undergoes a plastic deformation under suitable external load. This load can be applied either manually or through a machine. Metal forming processes can be classified as conventional metal forming and high strain rate forming.

1.1.1 Conventional Metal Forming

In conventional metal forming, the material is subjected to the strain varied from 0.1 to 5 s^{-1}. A punch and die system is used to deform the material into particular shape. Some typical examples of conventional metal forming methods include rolling, coining, extrusion and drawing.

1.1.2 High Strain Rate Forming

High strain rate forming methods are distinct from the conventional metal forming processes as the workpiece is accelerated to high kinetic energy, which is dissipated as plastic deformation to form the material. The strain rate of order 10^3 s^{-1} has been achieved during these processes. Some typical examples of high strain rate forming processes include methods such as electromagnetic forming, electrohydraulic forming, and explosive forming. Although high strain rate forming methods have been researched for over 100 years, the interest in these methods has increased in recent years due to their advantages such as improved formability and reduced springback over conventional metal forming processes. Over the past few years, there is an increase in interest to use aluminium to replace steel, especially in automobile sectors. The prime motive for aluminium use is to reduce the weight, which results in better fuel efficiency. However, formability of aluminium is lower than that of steel due to low strain hardening coefficient [1]. Also, springback is more severe in the case of aluminium as compared to steel due to low modulus of elasticity [2]. The formality of aluminium can be improved by utilizing high strain rate forming methods. Some of the typical high strain rate forming methods such as explosive forming, electrohydraulic forming, and explosive forming are discussed in the following text.

1. **Explosive Forming**
   The explosive metal forming process is a high strain rate forming process in which chemical energy of explosives is used instead of punch. Common explosives used in explosive forming are trinitrotoluene, cyclonite, and pentolite. Explosive forming can be categorized as contact and standoff type. In contact type, the explosive is in contact with the workpiece. In the case of standoff type, the workpiece is clamped over a die, and the assembly is placed into a container filled with water. The explosive material is placed at some distance from the workpiece as shown in Figure 1.1. As the explosive is fired, a shock wave of the high-intensity pressure wave is produced in water. When the high-intensity pressure wave strikes against the workpiece, the metal is formed into the die. Explosive forming requires long setup time, and it is suitable for the production of unique, low volume products [3].

2. **Electrohydraulic Forming**
   Electrohydraulic forming is a high strain rate forming process in which electrical energy is converted into mechanical energy. A pulse of high current is passed through two electrodes placed apart placed in a container filled with fluid as shown in Figure 1.2. The pulsed electric discharge vaporizes the fluid

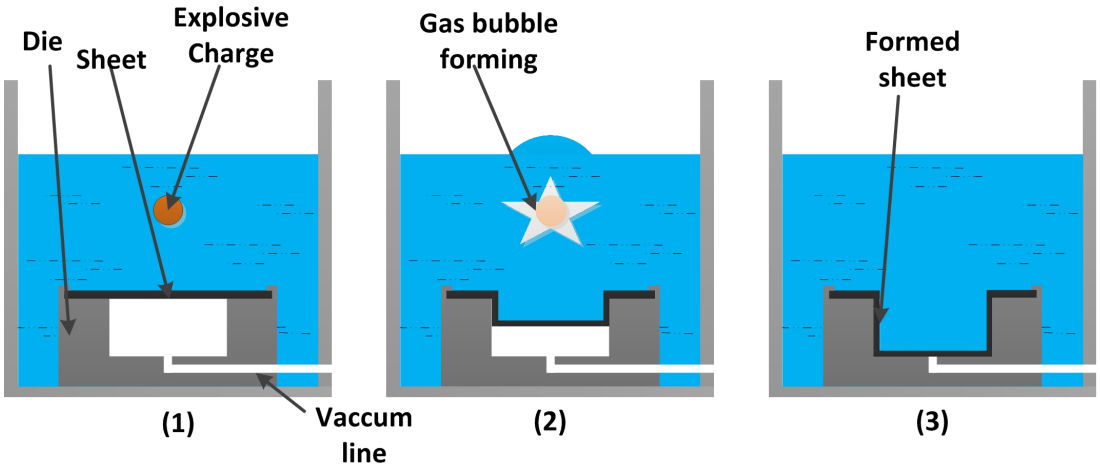

Figure 1.1: Explosive forming

around the electrode, thereby creating a shock wave. The shock wave moves away from the electrodes towards the workpiece. The shock wave impinges on the workpiece and deforms it into a die [4].

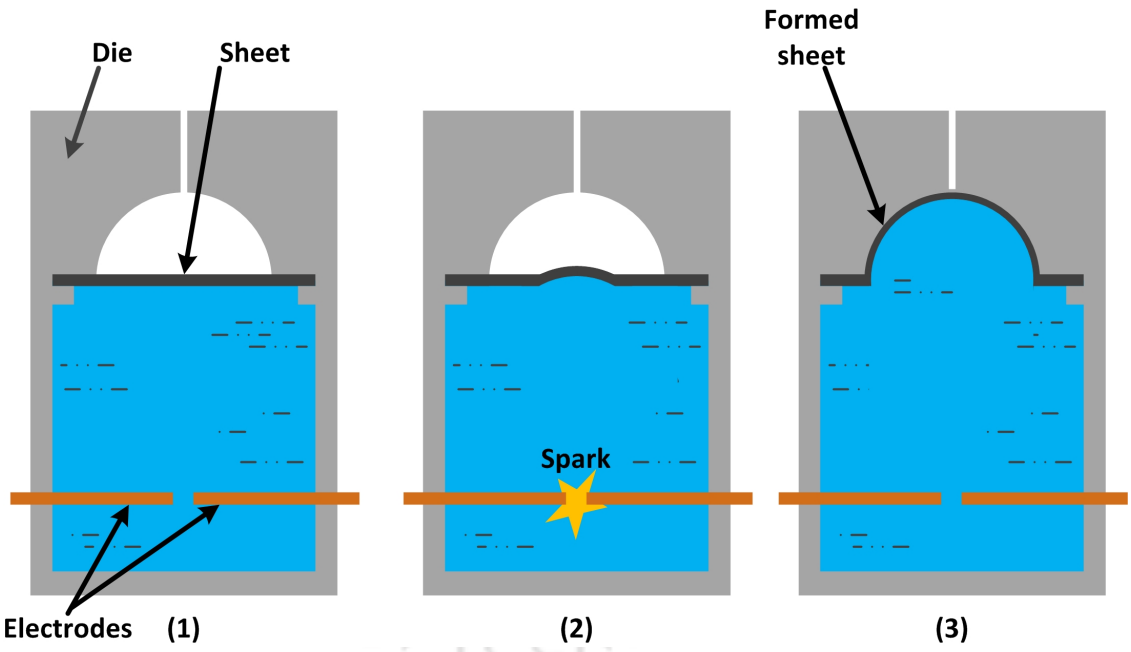

Figure 1.2: Electrohydraulic forming

3. **Electromagnetic Forming**
   In electromagnetic forming (EMF) process, a metal workpiece is forced into a die or free formed by a transient magnetic pressure. An electromagnetic forming system consists of three main parts: a capacitor bank, a coil, and a workpiece. In electromagnetic forming, the capacitor bank is used to store and discharge energy to make a pulsed current to flow through the coil. In EMF, the coil replaces the punch as in conventional forming to get the

desired deformation. The coil is connected to the capacitor that is charged and discharged in very short time. A transient magnetic field is produced by passing a sinusoidal damped electric current through a forming coil. The transient magnetic field produced by the coil induces eddy currents in the work-piece. The eddy currents flowing through workpiece produce their own magnetic field and restrict the penetration of coil magnetic field. The magnetic field of the workpiece is of opposite nature as produced by the coil. Due to the opposite nature of magnetic fields, repulsion force between the coil and workpiece results in forming of the workpiece. The process of electromagnetic forming is illustrated schematically in Figure 1.3.

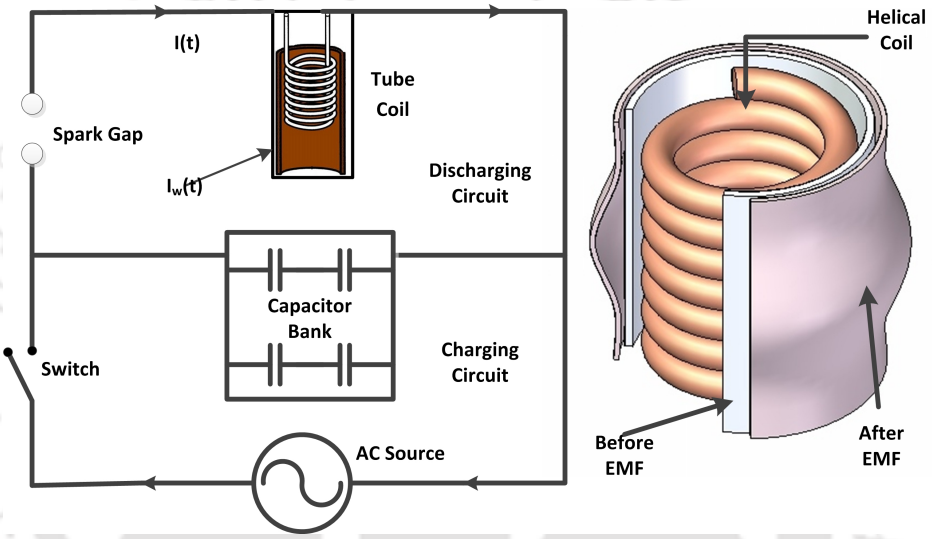

Figure 1.3: Electromagnetic forming

In Figure 1.3, discharging of capacitor bank results into the flow of time-varying primary current $I(t)$ through the forming coil. The time-varying primary current flowing through the forming coil produces a transient magnetic field, which interacts with the workpiece and induces the eddy currents $I_w(t)$ in the workpiece. Due to the opposite nature of the electric current flowing through the forming coil and workpiece, they repel each other. The repulsive Lorentz force so produced forms the workpiece into the desired shape using die. The electromagnetic forming system can be considered as an RLC circuit [5]. The current discharged by the capacitor bank through the coil can be obtained by solving RLC circuit equations as given by

$$L_c \frac{\partial I_c(t)}{\partial t} + M \frac{\partial I_c(t)}{\partial t} + R_c I_c + \frac{1}{C} \int I_c(t) dt = 0 \tag{1.1}$$

$$\frac{\partial \left(L_w I_w \right)}{\partial t} + \frac{\partial \left(M I_c \right)}{\partial t} + R_w I_w = 0 \tag{1.2}$$

where L_c the total inductance of the coil and the capacitor bank, M is the mutual inductance between the coil and the workpiece, $I_c(t)$ and $I_w(t)$ are the currents flowing through the coil and the workpiece, R_c is the total resistance of the coil and the capacitor bank, C is the capacitance of capacitor bank, L_w and R_w are the inductance and resistance of the workpiece. Inductance and resistance of the coil can be determined from geometry and material used for coil [6]. The inductance of spiral coil with N turns can be found out as

$$L = N^2 r \mu_0 \mu_r \left[\ln \left\{ \frac{8l}{a} - 2 \right\} \right] \tag{1.3}$$

where r is the radius of the coil, μ_0 and μ_r are absolute and relative permeability respectively, l is the length of the coil and a is the coil wire radius. The inductance of N turns solenoid coil is given by

$$L = \frac{\mu_0 N^2}{l} \left[\frac{A_0}{1 + \frac{A_i}{A_0}} \right] \tag{1.4}$$

where A_0 is the sectional area of the coil, A_i is the cross-sectional area of the wire, and l is the length of the coil. Resistance of the coil represents its resistance to flow of current, and the resistance of coil can be calculated by

$$R = \rho \frac{l}{A} \tag{1.5}$$

where ρ is the resistivity of coil material, l is the length of the coil and A is the area of wire.

On solving Eq. (1.1) and Eq. (1.2) with initial voltage of V_0 and current $I(0) = 0$, the current through the coil is given by

$$I_c = \frac{V_0}{\omega L} e^{-\beta t} \sin(\omega t) \tag{1.6}$$

where β is a damping coefficient, ω is the frequency. The current flowing through the coil creates a magnetic field. As the workpiece is inductively coupled to the coil, eddy current starts flowing in the workpiece. The penetration of eddy current in the workpiece is known as skin depth given by

$$\delta = \sqrt{\frac{2\rho}{\mu_0 \omega}} \tag{1.7}$$

where ρ is the resistivity of the workpiece material, μ_0 is the absolute permeability.

Applications of electromagnetic forming can be categorized as tube expansion, tube compression, and sheet forming. Tube expansion and compression operation consist of a helical coil placed inside and outside the tubular workpiece. A die can be used to give proper shape to the workpiece [7, 8]. The main application of electromagnetic forming is joining of axisymmetric components [9, 10]. Sheet forming operations consist of a spiral coil placed below the workpiece [11, 12]. Electromagnetic forming has also been utilized by some researchers to obtain axial form fit joints and torque joints [13, 14]. In the following chapters, electromagnetic forming has been studied.

1.2 Motivation

Due to increasing concern about global warming, there is an increasing need to improve fuel efficiency through decreasing vehicles weight. This can be achieved by utilizing lightweight materials for manufacturing. However, the light materials such as aluminium and magnesium were found to have lower formability. The high strain rate forming processes were found to increase the formability of light materials such as aluminium alloys. Therefore, electromagnetic forming as one of the high strain rate forming process is considered in the present work. Although electromagnetic forming has been known for decades, it's industrial use has risen in recent years. The electromagnetic field generated by coil acts as a tool in the electromagnetic forming and decides the magnetic pressure distribution with deformation of the workpiece. Based on the literature review the following research gaps are identified: 1. Previous work has only concentrated on the effect of a few process parameters during electromagnetic forming, but the effect of relative coil-tube length has not been analyzed in case of electromagnetic tube expansion. 2. The detailed study on the effect of frequency during electromagnetic forming has not been reported. 3. A fundamental issue during the electromagnetic forming is the low efficiency of the process and non-uniform distribution of the magnetic field. 4. It is not yet studied how the sheet will behave during the simultaneous forming and perforation of the sheet. The present work is in line with the identified research gaps.In the present study, the effect of coil-tube relative length during electromagnetic expansion has been analysed to show that different configurations lead to various tube geometries. As the current frequency is one of the critical parameters during electromagnetic forming, the effects of current frequency during electromagnetic tube expansion were analyzed by varying the

capacitance and thickness of the tube while keeping the energy constant. The optimum frequency is determined corresponding to the maximum deformation of the tube. The study shows that the optimum frequency depends upon the thickness of the tube for a particular material under study. To address the problem of low efficiency, improving coil and capacitor life during electromagnetic forming, the crow-barring of current pulse can be utilised. The idea of the crow-barring of current pulse originates from the fact that only a portion of the current pulse is responsible for forming and rest of the current pulse can be neglected. In the present study, the effect of crow-barring during electromagnetic forming is analysed by considering the maximum deformation of the sheet to find out the effective current pulse responsible for forming. In the present study, a feasibility study on electromagnetic forming and perforation of the sheet is performed to obtain an optimum energy to carry out the process. In summary, it is vital to study the effect of frequency, coil-tube length ratio during the electromagnetic tube expansion. There is little-reported literature on the crow-barring of the current pulse and its effect on workpiece deformation during electromagnetic forming. Also, there is no information regarding simultaneous forming and perforation of the sheet in the literature. So, the main motivation of the present research is to study the influence of parameters during electromagnetic forming and to establish the feasibility study on the electromagnetic forming and perforation of the sheet.

1.3 Objectives of the Research Work

The present work deals with the study of electromagnetic forming of tube and sheet, with its application to electromagnetic forming and perforation of sheets. The electromagnetic forming is investigated by carrying out experiments and validated with the finite element simulations. Objectives of the present research work are listed below:

1. Finite element modelling and simulation of electromagnetic forming of tubes and sheets
2. Experimental study of electromagnetic tube expansion and validation of finite element model
3. Parametric study of electromagnetic tube expansion
4. Parametric study of electromagnetic sheet forming
5. Coil design and die fabrication for electromagnetic forming and perforation of sheets

6. Experimental study of electromagnetic forming and perforation of sheets
7. Finite element modelling of electromagnetic forming and perforation of sheets

1.4 Contributions of the Work

The important contributions of the present work are listed below:

1. The experimental and finite element study of electromagnetic tube expansion has been performed to determine the influence of various parameters during electromagnetic tube expansion. The frequency range in which maximum tube displacement is obtained has been obtained.
2. Parametric study of electromagnetic sheet forming to determine the crowbarring effect during sheet forming.The simulation results show that only a part of the pulse is responsible for forming.
3. Feasibility study and optimization of electromagnetic forming and perforation of the sheet has been established.
4. Finite element modelling and simulation of electromagnetic forming and perforation of sheets has been performed to calculate the minimum velocity required for EMFP operation.

1.5 Organization of the Thesis

The thesis has been organized in seven chapters. A brief introduction to the chapters is given below:

Chapter 1 gives an introduction to various high strain rate forming processes such as explosive forming, electrohydraulic forming, and electromagnetic forming. It also presents the objectives and contribution of the present work with experimental setup used for the present study.

Chapter 2 presents the literature review of the electromagnetic tube and sheet forming. It provides the brief details of experiments and modelling studies performed by various researchers in the area of electromagnetic forming.

Chapter 3 gives details about experimental setup and the methodology to study electromagnetic forming of tube and sheets. It also discusses the measuring of

discharge energy using a Rogowski coil.

Chapter 4 is concerned with the experimental study of the electromagnetic expansion of tubes and validation of finite element model. Effect of various parameters such as coil length, discharge energy, coil pitch etc. during electromagnetic tube expansion is presented in this chapter.

Chapter 5 presents the parametric study of electromagnetic sheet forming. The effect of various parameters during electromagnetic sheet forming has been studied.

Chapter 6 deals with the coil and die design for electromagnetic sheet forming and perforation. It also presents the finite element modelling and simulation of electromagnetic forming and perforation of the sheet. It also presents the influence of discharge energy during electromagnetic sheet forming and perforation.

Chapter 7 concludes the present research work and defines the scope of future work.

CHAPTER 2

Literature Review

In this chapter, a detailed review of available literature on electromagnetic forming is carried out. Both experimental and numerical studies are investigated. The latest developments and trends of electromagnetic forming are discussed in the review by Psyk et al. [15], Mamalis et al. [16]. They studied the electromagnetic forming in a broad way. Discussion on both electromagnetic tube and sheet forming with the numerical and experimental investigation is presented. For the analytical investigation of electromagnetic forming, an equivalent circuit analysis is presented. It is shown by Psyk et al. [15] that workpiece motion affects the magnetic pressure, due to change in mutual inductance as the workpiece deforms. The two factors responsible for temperature rise during electromagnetic forming are plastic deformation and Joule heating. In the following sections, electromagnetic tube forming and electromagnetic sheet forming are discussed both experimentally and numerically.

2.1 History

The deformation of material utilizing magnetic field was first observed by Kapitza in 1924 [17]. The electromagnetic forming machine was patented by Harvey and Brower in 1961 [18] and was investigated in-depth during 1960's. After that research on electromagnetic forming was suddenly taken a break due to unavailability of high-performance equipment as well as computational facilities.

In the recent years, there is an increase in interest towards electromagnetic forming. The main driving force is to reduce the weight of automobiles that further results in fuel savings. A pulsed current through the forming coil produces a changing magnetic field. If the workpiece comes in exposure to the magnetic field, eddy current starts flowing in the workpiece due to changing magnetic field. The strength of induced eddy current depends upon the rate of change of magnetic field and conductivity of the material. The induced eddy current produces its own magnetic field, whose direction is opposite to that of the magnetic field

around the coil. This results in the Lorentz force acting on the workpiece to plastically deforms it. More the strength of the induced magnetic field, the more will be the shielding of the magnetic field and the more will be the workpiece deformation [19, 20].

2.2 Equipment and Material

The electromagnetic forming system mainly consists of a capacitor bank, a forming coil, and a field shaper as discussed in the following section.

2.2.1 Capacitor Bank

The high voltage energy during electromagnetic forming is provided by the capacitor bank which consists of capacitors connected in series and parallel. The capacitor bank stores energy and then releases it through the forming coil. The capacitor bank is connected to the forming coil through the high voltage switches (ignitron type or solid state silicon controlled rectifier). The energy storage of the capacitor bank is given by

$$E = \frac{CV^2}{2} \tag{2.1}$$

where C is the capacitance, and V is the charging voltage of the capacitor bank. The parameters of the capacitor bank are chosen in such a way that it maximizes the life and minimizes the operational cost of the machine. The suitable capacitor bank should have minimum self-inductance and ability to withstand a large number of pulse discharges. During electromagnetic forming, only first one or two pulses are responsible for forming. A capacitor bank with energy capacity 5 to 80 kJ is used for electromagnetic forming.

2.2.2 Forming Coil

The forming coil acts as a tool in electromagnetic forming. The coil geometry depends upon the forming operation. The coil is designed in a way to transfer the maximum of stored energy to the workpiece.

1. **Single Turn Coil**
   Single turn coils are the simplest form of coils, which are made by cutting a plate of conductive material [21]. A single turn compression coil is shown in Figure 2.1.

2. **Multi Turn Coil**
   Multi-turn coils are produced by wrapping a conductive wire in a particular

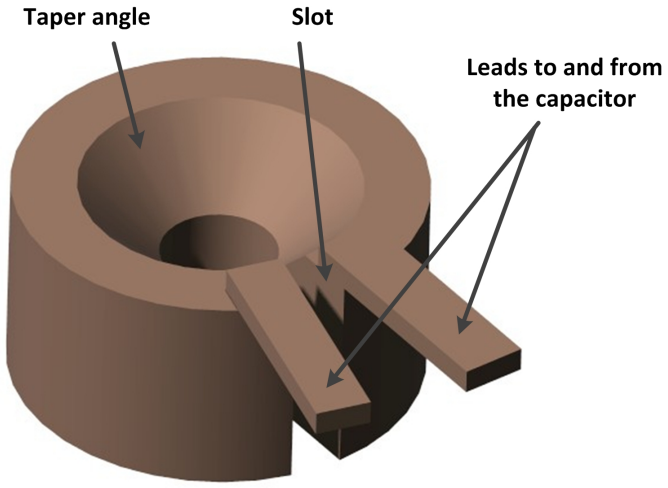

Figure 2.1: Single turn coil

pattern. In general, there are three types of coils: helical coil for compression, helical coil for expansion and spiral coil for sheet forming as shown in Figure 2.2.

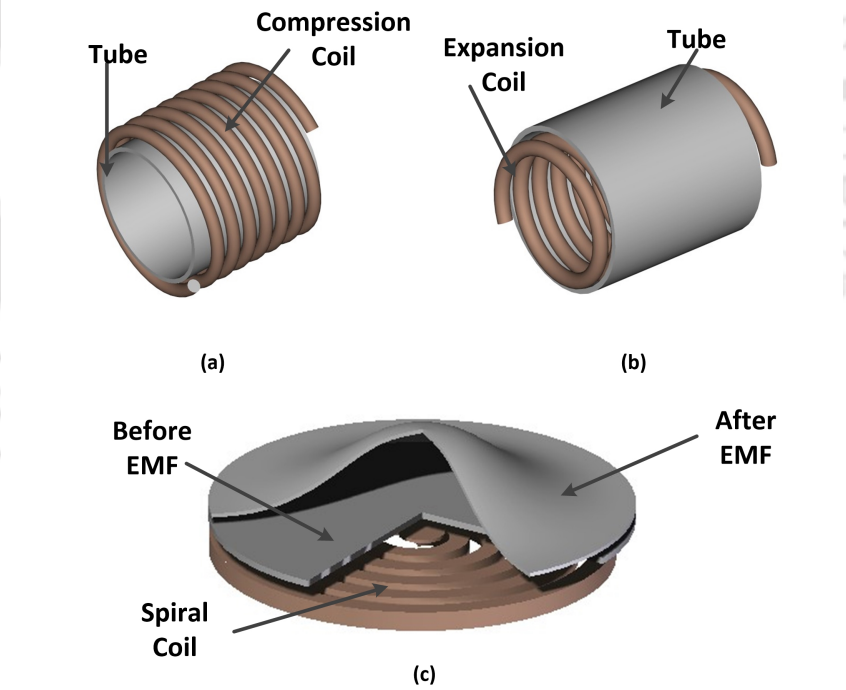

Figure 2.2: Electromagnetic forming coils (a) Helical coil for tube compression (b) Helical coil for tube expansion (c) Spiral coil for sheet forming

In multi-turn coils, strength is an important factor during coil design [22]. Wires of multi-turn coils should be of high conductivity and high strength material. Copper as a coil material is well qualified if only electrical conductivity is considered as it has low mechanical strength. Some examples of stronger coil materials are zirconium, tungsten, beryllium bronze and cad-

mium copper [23]. In multi-turn spiral coils, pressure distribution is non-uniform, so a uniform pressure actuator was designed by Kamal et al. [24]. Golowin et al. [25] used the uniform pressure actuator to form fine surface features on sheet metals.

2.2.3 Field Shaper

Field shapers are used to direct the magnetic flux to the desired area to deform the workpiece. A forming coil is used to induce the current in field shaper. A field shaper for tube compression is shown in Figure 2.3. The efficiency of the forming gets reduced by using the field shaper [26].

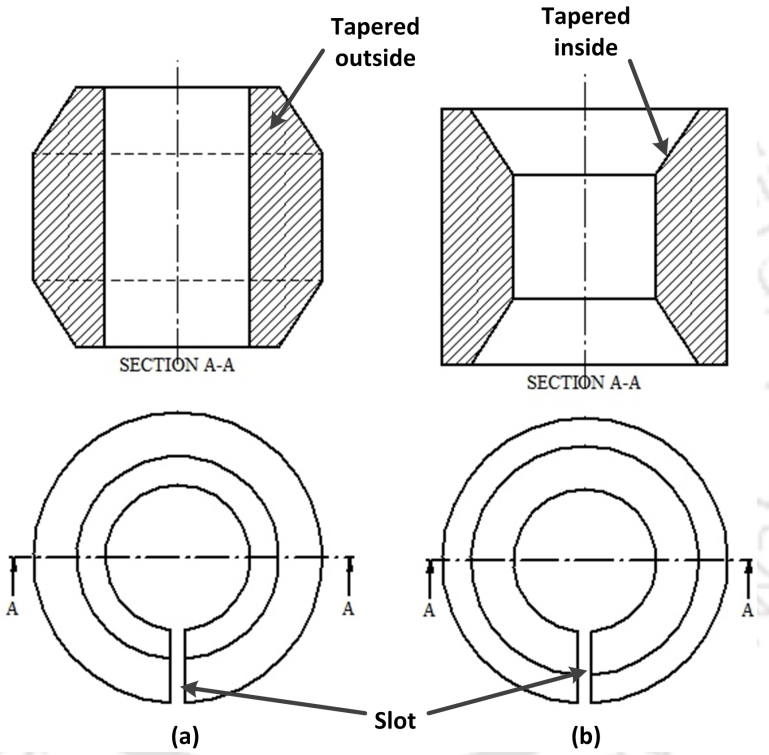

Figure 2.3: Field shaper (a) For tube expansion (b) For tube compression

Figure 2.3 shows the field shaper for electromagnetic tube expansion and compression. The flow of current through the coil produces the magnetic field that interacts with the field shaper. The coil magnetic field induces the current in the field shaper, which starts flowing on the surface of the field shaper. The field shaper surface near to the workpiece acts as a forming coil and produces its own magnetic field. As the workpiece is inductively coupled to the field shaper, it results in the flow of eddy current in the workpiece due to induction. Due to the opposing nature of the magnetic field, a repulsive force is generated that results in forming of the workpiece [27].

2.2.4 Die

To obtain the desired shape of the workpiece, a die can be used. If a high conductive material is used for die, eddy currents can also flow in the die. The eddy current flowing through the die produces a damping effect, resulting in incomplete filling of die [28]. Another issue of using the die in electromagnetic forming is sparking between the die and the workpiece. Therefore, epoxy-based materials are generally used to manufacture dies for electromagnetic forming.

2.2.5 Workpiece

A high conductive material is desirable for electromagnetic forming such as copper, aluminium, low-carbon steel, gold, silver and brass. High electrical conductive materials can be formed using low-frequency discharge circuit. The less electrical conductive materials can be formed using driver material [29]. As the basic working of electromagnetic forming is based on magnetic field and induced current, the workpiece should provide continuity to the flow of induced current. If the workpiece has slits and number of holes in it, the forming pressure get lower down and decreases the efficiency of forming. Another important characteristic is the thickness of the workpiece. The upper limit of workpiece thickness depends on the energy capacity of the electromagnetic forming machine and the coil strength. The lower limit of the workpiece thickness is determined by the skin depth and shielding behaviour [30, 31].

2.3 Electromagnetic Tube Forming

Song et al. [32] studied the distribution of magnetic pressure as the relative coil-workpiece axial position is varied. A 14 kJ electromagnetic forming system and aluminium tube as tube material is used by Song et al. [32] to carry out the experiments. It is shown by Song et al. [32] that a variety of tube shapes can be produced by varying the relative coil-workpiece axial position. This is due to the change in magnetic pressure distribution as the relative coil-workpiece axial position is varied.

Zhang et al. [33] studied the effect of various parameters during electromagnetic expansion. Zhang et al. [33] modelled the electromagnetic forming and validated it with experimental results. By varying the working parameters, a variety of tube profiles is obtained. By performing experimental and numerical studies, a set of optimal working parameters is obtained. Yu and Li [34] focused on the effect of coil length during tube compression. They investigated the effect of coil length on magnetic pressure and tube deformation. Both experimental and numerical

analysis are used to study the influence of the coil length during tube compression. For experiment aluminium tubes and three coils of different lengths were used. Studies on wrinkling during electromagnetic forming was investigated by Padmanabhan et al. [35]. To study the wrinkling, ring compression electromagnetic forming tests were performed. They investigated the effects of ring height, ring thickness, material, and energy. They observed that as the energy increases, the tendency for wrinkling decreases. For a constant energy, the tendency for wrinkling decreases as the ring thickness or ring height increases.

2.4 Electromagnetic Sheet Forming

Al-Hassani et al. [36] studied the electromagnetic sheet forming by using four types of spiral coils to form aluminium sheets on a die having holes. By measuring the height of the dimples formed, magnetic pressure distribution were predicted. Al-Hassani et al. [36] also calculated the magnetic pressure distribution analytically for electromagnetic sheet forming.

Takatsu et al. [37] studied the electromagnetic sheet forming using aluminium sheets. A five-turn copper spiral coil was used to perform the experiments. A high-speed photographic imaging was used to measure the displacement of the workpiece. It was observed that the deformation of the sheet at centre starts later than at the circumference, which is due to the non-uniformity of magnetic pressure.

Imbert et al. [38] studied the influence of tool-sheet interaction on the formability of sheet. The sheet was formed freely and by using a conical die. Strain measurement was used to know the influence of tool-sheet interaction on the formability. The experiments by Imbert et al. [38] show that the formability of the sheet got increased by using the conical die, especially at areas where die-sheet contact takes place.

Padmanabhan et al. [35] focused on the ways to control the wrinkling and springback during electromagnetic sheet forming. Various parameters are examined to know their effect on springback and wrinkling. Padmanabhan et al. [35] show that the wrinkling decreases with the increase in magnetic pressure. For a constant discharge energy, wrinkle decreases with the increase in sheet thickness.

Risch et al. [39, 40] studied the effect of workpiece stiffness during the electromagnetic sheet forming and proposed die design to locally increase the stiffness of sheet to handle the rebound effect. In electromagnetic forming due to the high speed of workpiece, the kinetic energy of workpiece is not completely transferred into plastic deformation in the small amount of time. When the workpiece comes in contact with the die, the excess kinetic energy results into rebound effect.

Cao et al. [41] proposed a discharged circuit to crow-bar the current pulse thereby reducing the overheating of the coil. Electromagnetic force during electromagnetic forming decreases with increase in distance between the coil and the workpiece. To overcome this difficulty, Li [42] proposed an axially movable electromagnetic forming system to deform a large metallic sheet.

Hartmann et al. [43] proposed a 100 kJ electromagnetic forming machine to deform large sheet. Formability of sheet during electromagnetic forming was studied by Seth et al. [44]. The formed sheets were used to plot forming limit diagram. Oliveira et al. [45] performed electromagnetic forming experiments to compare cavity fill forming and free forming. A flat double spiral coil and two aluminium alloys AA 5574 and AA 5182 were used to perform the experiments. Oliveira et al. [45] concluded that formability doesn't get increased by electromagnetic forming as depicted by forming limit diagram.

2.5 Advantages of Electromagnetic Forming

Some of the advantages of electromagnetic forming process are listed below:

1. **Improved Formability :** A product can be formed successfully, if material tearing, springback, and wrinkling tendency of material can be avoided. Wrinkling and springback can be avoided by providing a minimum amount of stretching to the material. The upper limit of stretching is decided by the material tearing strength. Thus, the successful forming of material is restricted by necking on one hand and springback and wrinkling on the other hand. The forming limits in conventional forming are often small. The electromagnetic forming is found to increase the forming limit of material [46]. In EMF, the velocity of the workpiece achieved is 100 to 1000 times higher than the conventional forming. The high-velocity deformation can significantly increase the strain at which failure occurs due to inertia effect [47, 48]. Several results from the literature indicate that electromagnetic forming reduces wrinkling and springback [49, 50].

2. **Capturing of Fine Details :** The large pressures during the electromagnetic forming can be used to capture fine surface details. Electromagnetic forming can be used for coining operations [51].

3. **Punch-less Process :** As the electromagnetic forming is a punch-less process, tooling costs get reduced. As the electromagnetic forming is a non-contact forming process, surface finishing operations can be performed before forming [52].

4. Electromagnetic forming can lead to high productivity if automated as the operation time is around 200 µs.

5. As the electromagnetic forming reduces springback, close dimensional tolerances can be provided to the product.

2.6 Limitations of Electromagnetic Forming

1. As only small part of charging energy is used for plastic deformation, process efficiency is as low as 2 to 20 %.

2. As process involves large currents, it requires significant safety measures and skilled operators.

3. Tool life is low.

4. Cost of initial setup is high.

5. Deep drawing is not easily possible with EMF.

6. Materials to be formed should have high electrical conductivity.

7. Only relatively thin-walled components can be formed electromagnetically.

CHAPTER 3

Electromagnetic Tube Expansion

3.1 Introduction

To understand the effect of various process parameters during electromagnetic forming, tube and sheet electromagnetic forming experiments were performed. The FE results were validated with the experimental results. This chapter is focused on the study of various parameters on the magnetic pressure distribution and workpiece deformation during electromagnetic forming.

3.2 Experimental Setup

The experiments were carried out using a 10 kJ electromagnetic forming machine with a 90 µF capacitance of capacitor bank that can be charged up to 15 kV. The experimental setup is shown in Figure 3.1.

Figure 3.1: Electromagnetic forming system

The electromagnetic forming system consists of following components:-

1. **Energy Storage Unit:** The energy storage unit consists of two capacitors, each of 45 µF capacitance, connected to a high voltage switch. The capacitors are charged by using a high voltage power supply. The capacitors are connected in parallel to give the total capacitance of 90 µF for capacitor bank. The energy storage for the capacitor bank is given by

$$E = \frac{CV^2}{2} \tag{3.1}$$

where E is the stored energy, C is the capacitance and V is the applied voltage across the capacitor bank.The energy discharged by capacitor bank can be control using control unit. An ignitron switch is used to discharge the high voltage energy from the capacitor bank to the coil

2. **Control Unit:** The control unit consists of control system with a display unit and a transformer. The transformer is to charge the capacitor at high voltage. The voltage at which the capacitor has to be discharged is controlled by the control system. The control unit displays the energy at which the capacitor bank has to discharge through the coil, for performing the electromagnetic forming operation. When the discharge switch is pressed, high voltage switch makes the capacitor bank to discharge current through the coil.

3. **Coil:** The coil is used to transfer energy to the workpiece using the mutual inductance between the coil and the workpiece. As the coil carries high voltage current, the coil turns are properly insulated to avoid the spark between them. According to the forming operation, a suitable coil geometry is selected. Two types of coils namely helical and spiral coil are generally used as shown in Figure 3.2.

4. **Measurement Unit:** The measurement unit consists of a Rogowski coil, an integrator and an oscilloscope. The Rogowski coil is an alternating current measuring device. It is based on the principle of Ampere's law and Faraday's law. It consists of a helical coil wrapped around a lead wire. The conductor for which current has to be measured is placed at the centre of the Rogowski coil. The current flowing through the conductor produces a magnetic field and induces a voltage in the Rogowski coil by mutual induction. The Rogowski coil voltage is proportional to the rate of change in the current through the conductor. The Rogowski coil is connected to the

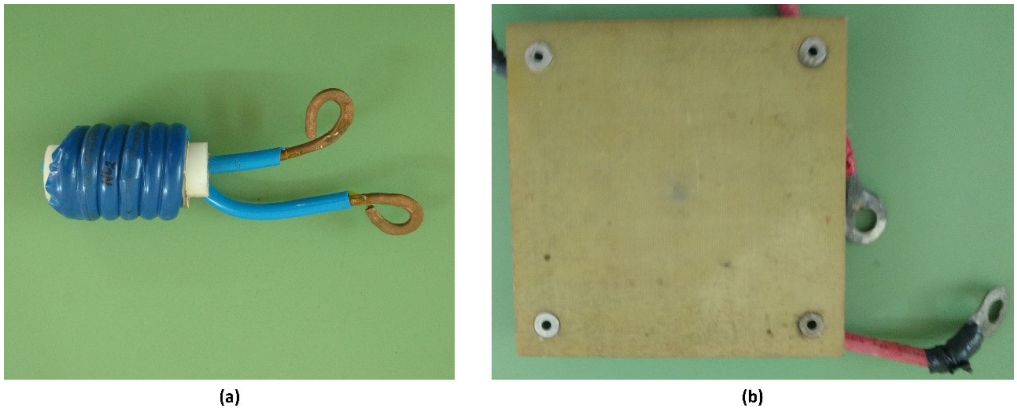

Figure 3.2: Electromagnetic forming coil (a) 6 turns helical coil (b) 7 turns Spiral coil enclosed inside epoxy casing

integrator to provide the voltage proportional to the current. The Rogowski coil with the integrator is shown in Figure 3.3.

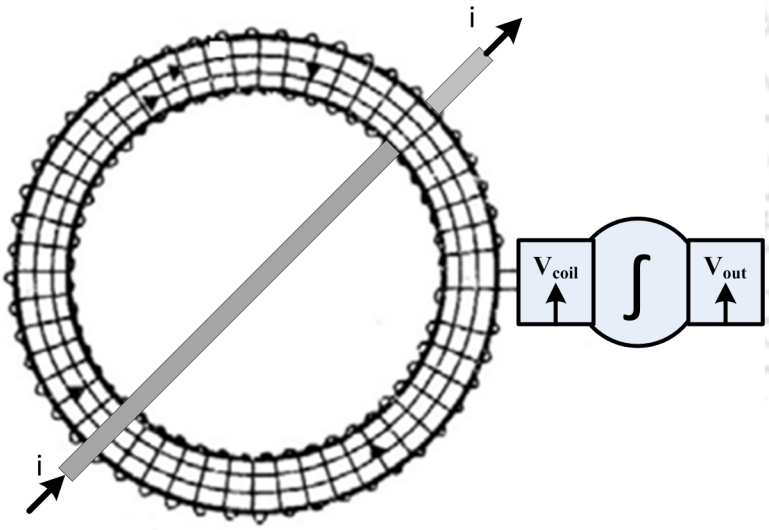

Figure 3.3: Rogowski coil with integrator

The voltage (V_{coil}) induced in the Rogowski coil is given by

$$V_{coil} = -M\frac{\partial i}{\partial t} \tag{3.2}$$

The induced voltage in the Rogowski coil is proportional to the rate change of current but to get the voltage proportional to the current, an integrator is needed. The integrator output voltage is given by

$$V_{out} = -\frac{1}{\tau}\int V_{coil}\partial t \tag{3.3}$$

where V_{out} is integrator voltage , τ is the integration time constant and V_{coil} is the Rogowski coil voltage. To display the current waveform an oscilloscope is used as shown in Figure 3.4.

Figure 3.4: Oscilloscope for current measurement

The output of the integrator is connected to the oscilloscope input channel. The oscilloscope was set for 1 V equal to 25 kA and trigger is set to edge type.

3.3 Tube Expansion

The material of the tube was AA 6061, of length 80 mm and 45 mm diameter with a thickness of 1.5 mm. Coils used for experiments were of copper material with a wire diameter of 4 mm. Three coils of 6, 10 and 14 turns were used to study the effect of various parameters during electromagnetic forming. The 6 turn coil has inductance of 0.98 µH with resistance of 3.3 mΩ, 10 turn coil has inductance of 1.849 µH with resistance of 5.63 mΩ, and 14 turn coil has inductance of 2.746 µH with resistance of 7.9 mΩ. The dimensions and parameters of the coils are tabulated in Table 5.4. The gap between the coil and tube is 1 mm. The distribution of magnetic intensity in the space between the coil and the workpiece depends on the factors such as length of the coil, pitch of the coil, gap between the coil and workpiece for the given energy. The distribution of the magnetic field intensity changes as the length of the coil is changed relative to the workpiece, which affects the tube deformation. Tube length was kept constant equal to 80 mm for all the experiments.

A damped pulsed current is the load during the electromagnetic forming. Only initial part of the current is responsible for the deformation. During electro-

Table 3.1: Coil parameters to study the effect of coil-tube relative length

Coil	Turns (No.)	Diameter (mm)	Inductance (µH)	Frequency (kHz)
C1	6	43	0.98	19.40
C2	10	43	1.85	14.12
C3	14	43	2.75	11.60

magnetic forming, the current is given by

$$I = V\sqrt{\frac{C}{L}}\exp(-\beta t)\sin(\omega t) \tag{3.4}$$

where V is the discharge voltage, C is the capacitance, L is the inductance, β is the damping exponent, and ω is the angular frequency.

The electromagnetic forming process is based upon Maxwell's equation. The Maxwell equations in terms of magnetic vector potential ($\vec{A}$) and electric scalar potential (φ) is given by Eq. (3.5 and 3.6).

$$\nabla \cdot \sigma\vec{\nabla}\varphi = 0 \tag{3.5}$$

$$\sigma\frac{\partial\vec{A}}{\partial t} + \vec{\nabla} \times \frac{1}{\mu} \times \vec{A}\sigma\vec{\nabla}\varphi = \vec{J_s} \tag{3.6}$$

The first equation states that divergence of electric field is zero. The second equation shows that the total current density $\vec{J_s}$ is equal to the sum of the current density due to the change in magnetic field (B) and the electric field (E).
With boundary conditions,

$$\vec{n} \cdot \vec{\nabla}\varphi = 0 \text{ on } \Gamma \tag{3.7}$$

$$\varphi = \varphi \text{ on } \Gamma_c \tag{3.8}$$

Where, σ is the conductivity, $\vec{J_s}$ is the current density in the tube, μ is the permeability, Γ represents the surface of the coil and tube, Γ_c represents the region where the coil is connected to the external current supply. The equation (3.7) states that the gradient of the electric potential is orthogonal to the surface normal ($\vec{n}$). The equation (3.8) shows that the potential at the coil current input surface is equal to the source potential.
Eq. (3.5 and 3.6) are solved by finite element method to calculate potentials $\vec{A}$ and φ. The calculated potentials are then used to calculate electromagnetic fields using Eq. (3.9, 3.10, and 3.11)

$$\vec{E} = -\vec{\nabla}\varphi - \frac{\partial \vec{A}}{\partial t} \tag{3.9}$$

$$\vec{B} = -\vec{\nabla} \times \vec{A} \tag{3.10}$$

$$\vec{J} = \sigma\vec{E} + \vec{J}_s \tag{3.11}$$

Once the electromagnetic fields are calculated, Lorentz force ($\vec{F}$) acting on the workpiece is calculated using Eq. (3.12)

$$\vec{F} = \vec{J} \times \vec{B} \tag{3.12}$$

The Lorentz force calculated is then substituted to the transient dynamic equilibrium Eq. (3.13)

$$M\ddot{u} + C\dot{u} + Ku = \vec{F} \tag{3.13}$$

Where M represents the structural mass matrix, C is structural damping matrix, u is the nodal displacement vector, K is the structure stiffness matrix, and F is the load vector. Figure 3.5 shows the relative tube and coil size used for electromagnetic tube expansion with the finite element mesh.

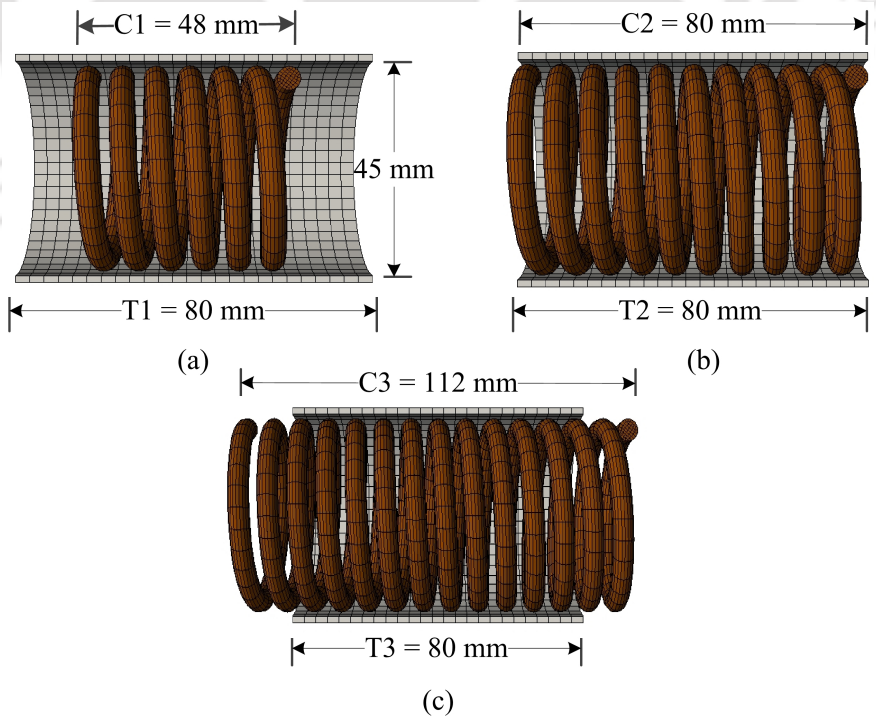

Figure 3.5: Coil-tube arrangement for coil (a) C1 (b) C2 (c) C3

The finite element mesh of tube and coil is shown in Figure 3.5. The tube and

Table 3.2: AA 6061 material constants for Johnson Cook constitutive model

Poisson's Ratio	0.33	**A** (MPa)	324
Density (kg/m^3)	2700	**B** (MPa)	114
Elastic Modulus (GPa)	68.90	**C**	0.002
Resistivity Ω.m	0.04	**n**	0.42
T_m (K)	925	**m**	1.34

coils are meshed using hexahedral elements with 2540 elements for the tube and 4230, 7050 and 9870 elements for the coil. As by increasing the number of elements, the error in finite element analysis decreases. Hence, the number of elements has been increased but the results remain the same.The current curves obtained from experiments are used as input to the electromagnetic tube simulation. The material of the coil is copper with the resistivity of 1.7×10^{-8} Ω/m. For the tube, Johnson-Cook material model was used as given by Eq. (3.14) with J-C parameters tabulated in Table 3.2. The coil was modelled as rigid.

$$\sigma_y = (A + B\bar{\varepsilon}^n)(1 + C\ln\dot{\bar{\varepsilon}})\left[1 - \left(\frac{T - T_R}{T_m - T_R}\right)^m\right] \tag{3.14}$$

where σ_y and $\bar{\varepsilon}$ are the equivalent plastic stress and plastic strain, $\dot{\bar{\varepsilon}}$ is the relative plastic strain rate, and T_R and T_m are room and melting temperature of material. A, B, C, m and n are material parameters obtained by mechanical testing.

3.4 Results and Discussion

In the following section, the experimental results of electromagnetic tube expansion were analysed and compared with the simulation results. The validated model is used to study the effect of various parameters during electromagnetic tube expansion.

3.4.1 Effect of Coil Length

Three coils of 6, 10 and 14 turns were used to study the electromagnetic expansion of tubes. Relative size is defined as the ratio of the coil to tube length. The current pulse can be easily measured using the Rogowski coil. The current curves obtained using coils C1, C2 and C3 are shown in Figure 3.6. The maximum current for coil C1, C2 and C3 are 112 kA, 92 kA, 82 kA respectively. As the coil length is increased, the inductance of the coil also increases and so the current curve frequency decreases.

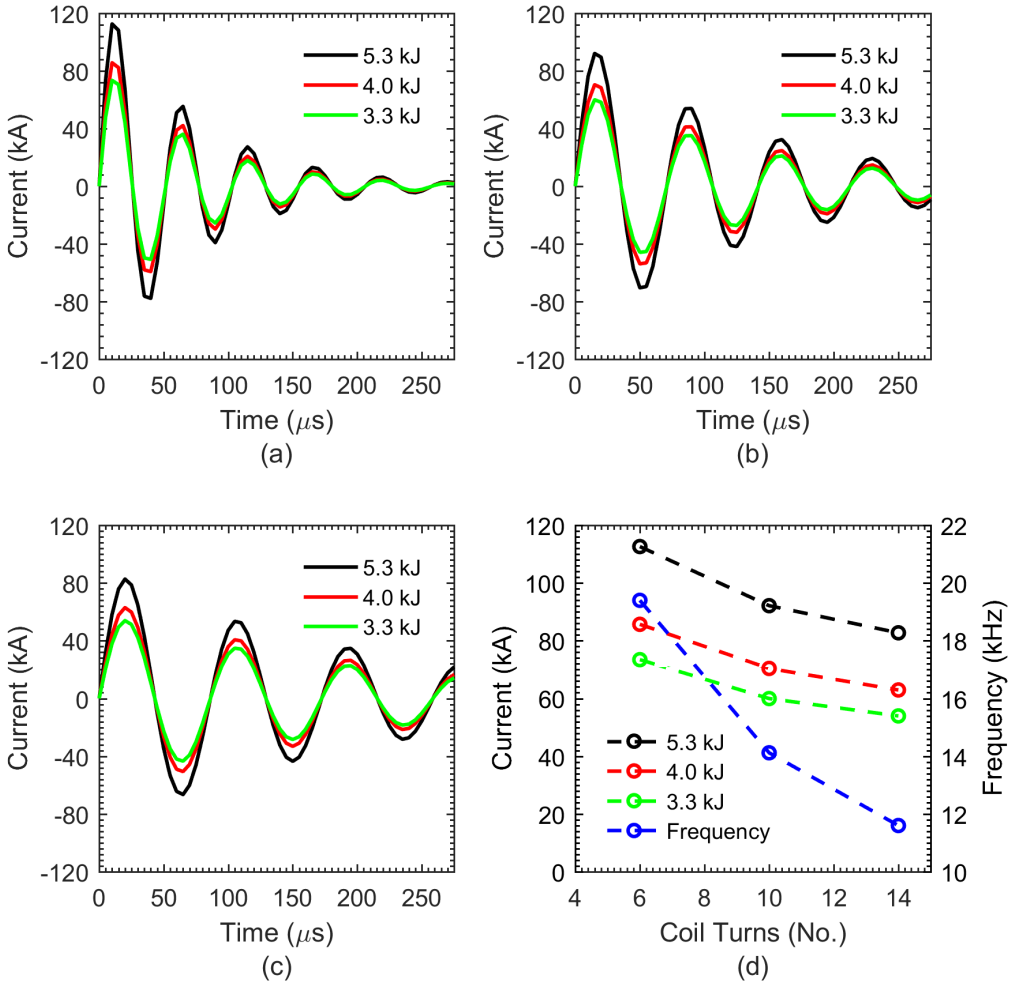

Figure 3.6: Current curve for coil (a) C1 (b) C2 (c) C3 (d) Effect of coil turns on maximum current and frequency

Deformed tubes obtained experimentally with simulated results are shown in Figure 3.7. In case of coil C1, the magnetic pressure is confined to the smaller region as coil length is smaller than the tube which results into tube bulged at centre shape. As coil length is increased to coil C2, a uniform bulged shape is obtained. For coil C3, the magnetic pressure at the tube ends is more than that at tube centre, resulting in flanged shape. Experimental results show that, in case of coil C1 (relative size less than 1), the radial displacement increases with increase in discharge energy with maximum radial displacement at tube centre. The radial displacement of the tube is non-uniform along the length with maximum radial deformation at the centre of the tube. In case of Coil C2 (relative size equal to 1), the radial deformation of the tube is more uniform along the length. In case of coil C3 (relative size greater than 1), the radial deformation of the tube is uniform along the length except at tube ends with maximum tube deformation at the tube

ends.

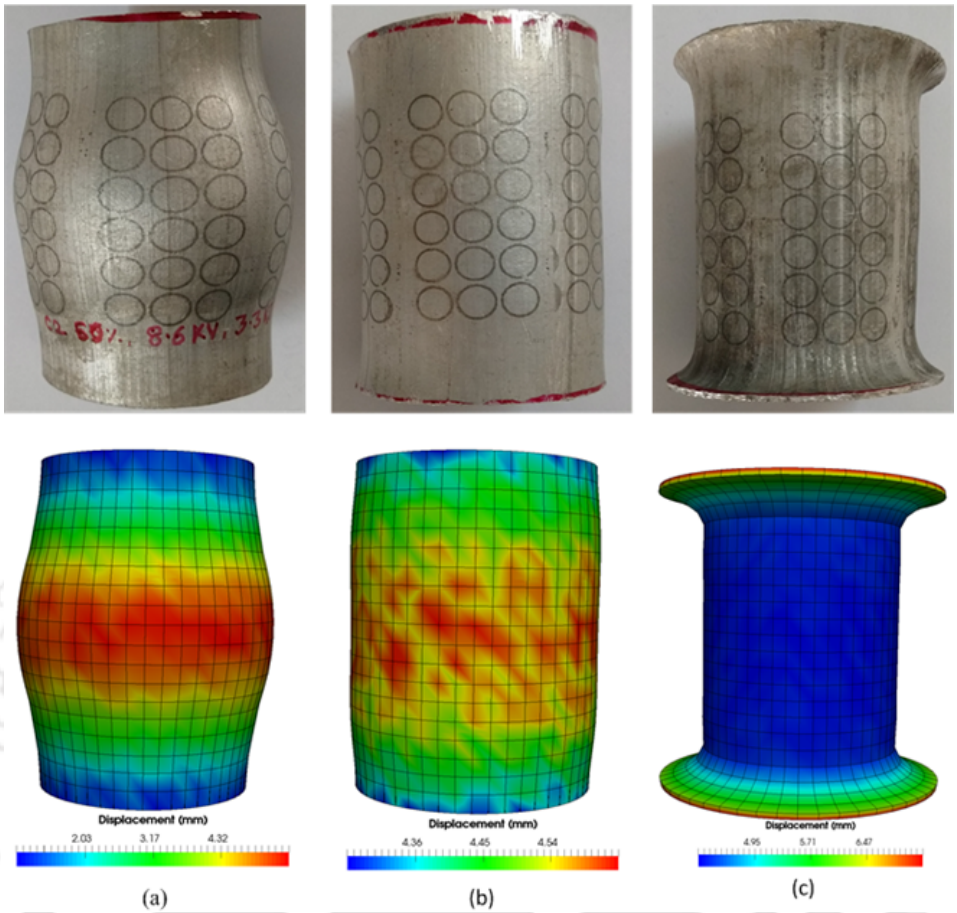

Figure 3.7: Comparison of electromagnetically deformed tubes with simulated results for coil (a) C1 (b) C2 (c) C3

The comparison between experimental and simulated tube displacement is shown in Figure 3.8, and a good agreement between them is observed. The simulation error was found to be about 6.4 %. The validated model is then used to know the effect of coil-tube relative length during electromagnetic tube expansion in the following section.

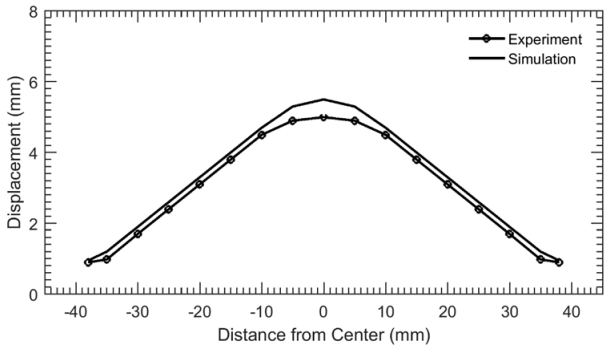

Figure 3.8: Comparison between experimental and simulated result

Figure 3.9 shows the deformed profile of tube with coil C1, C2 and C3 at discharge energy of 3.3 kJ, 4 kJ and 5.3 kJ respectively. The tube radius increases with the increase in discharge energy, the maximum tube displacement obtained for coil C1, C2 and C3 are 5 mm, 4.5 mm and 4.2 mm, respectively.

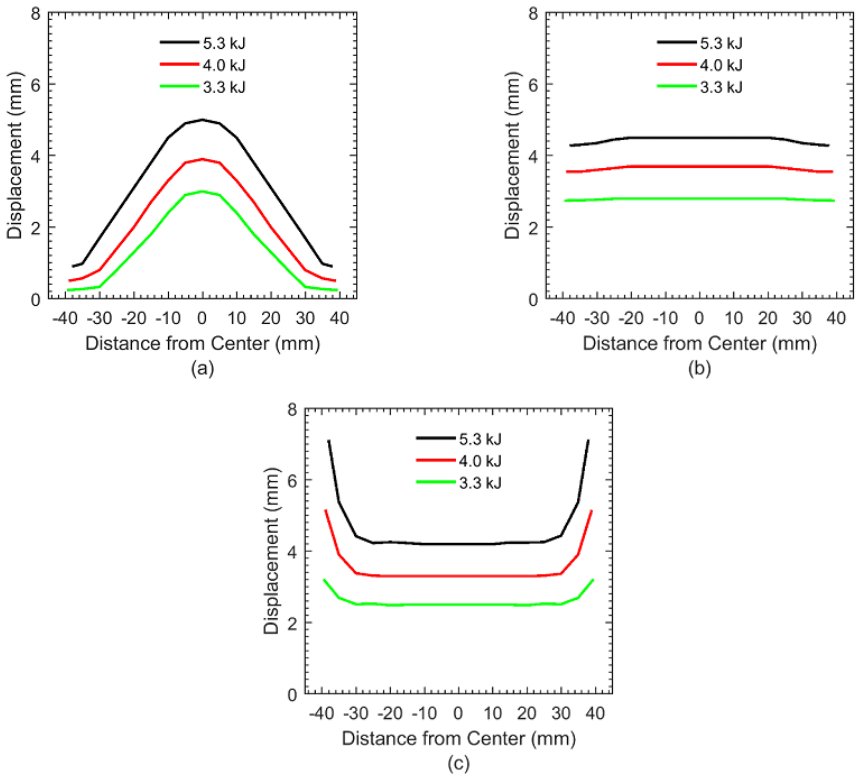

Figure 3.9: Deformed tube profile with coil (a) C1 (b) C2 (c) C3

The validated model is used to predict the magnetic pressure and its distribution. Figure 3.10 shows the effect of the relative size of the tube and coil on the magnetic pressure during electromagnetic tube expansion.

As the magnetic pressure is proportional to the current, magnetic pressure increases with increase in peak current. The damping coefficient of magnetic pressure also decreases with the decrease in damping coefficient of current. For coil C1, C2 and C3 the maximum pressure obtained are 20.2 MPa, 18.9 MPa and 13.4 MPa respectively. The simulated results of the magnetic pressure distribution using different coil lengths are shown in Figure 3.11.

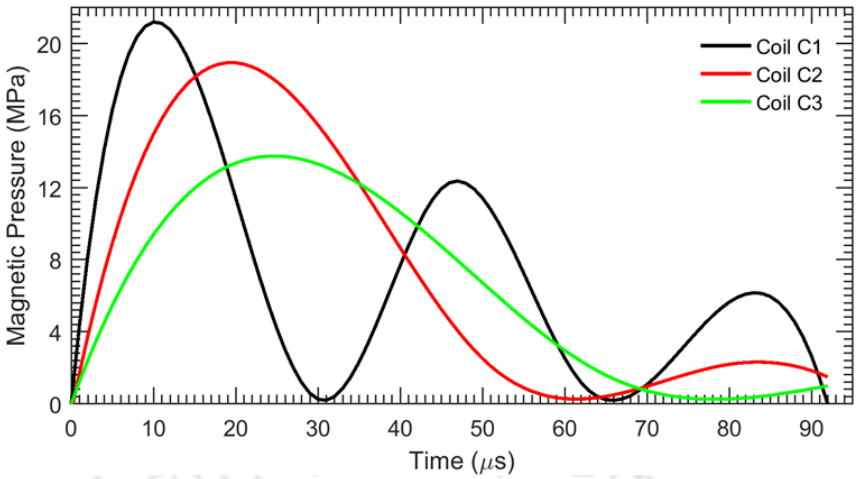

Figure 3.10: Magnetic pressure for coil C1, C2 and C3

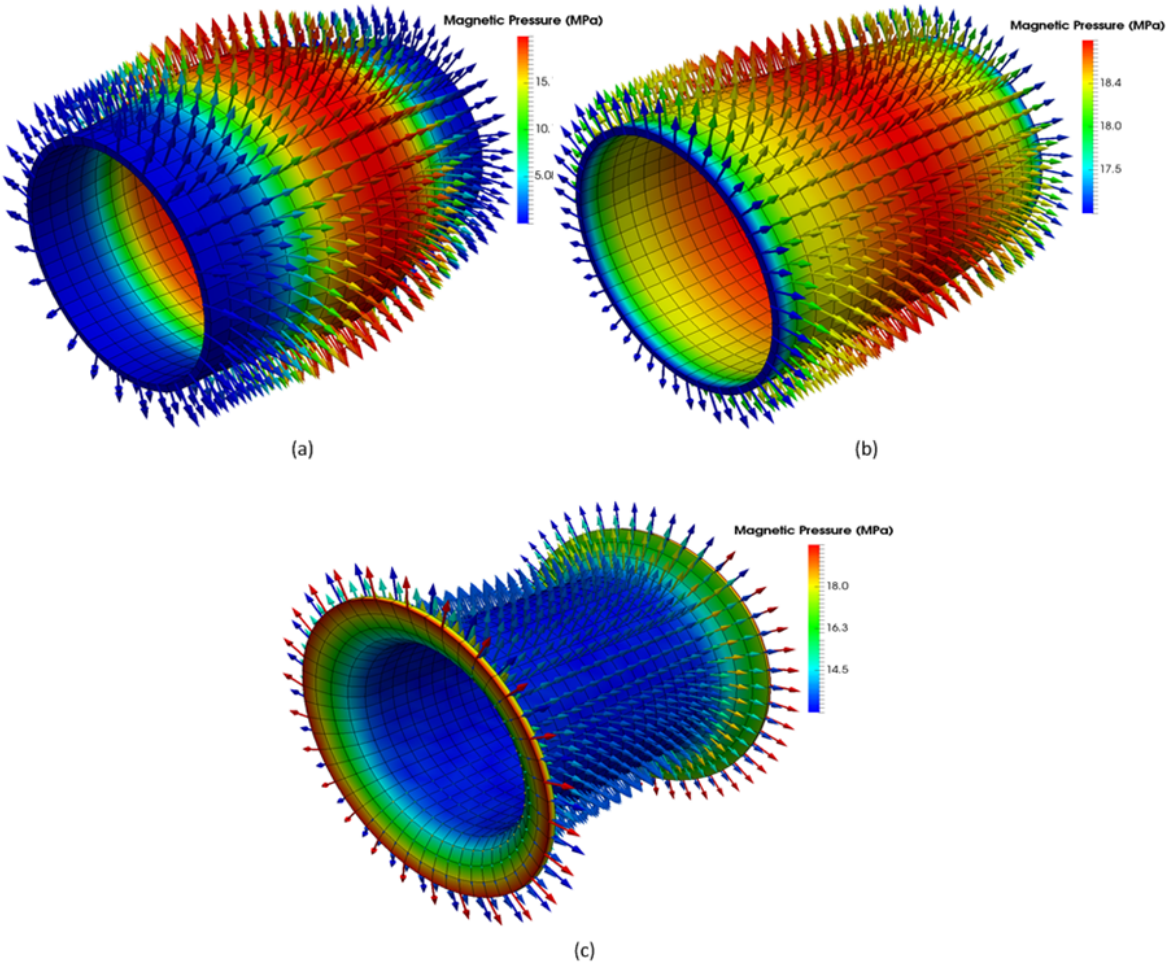

Figure 3.11: Magnetic pressure distribution for coil (a) C1 (b) C2 (c) C3

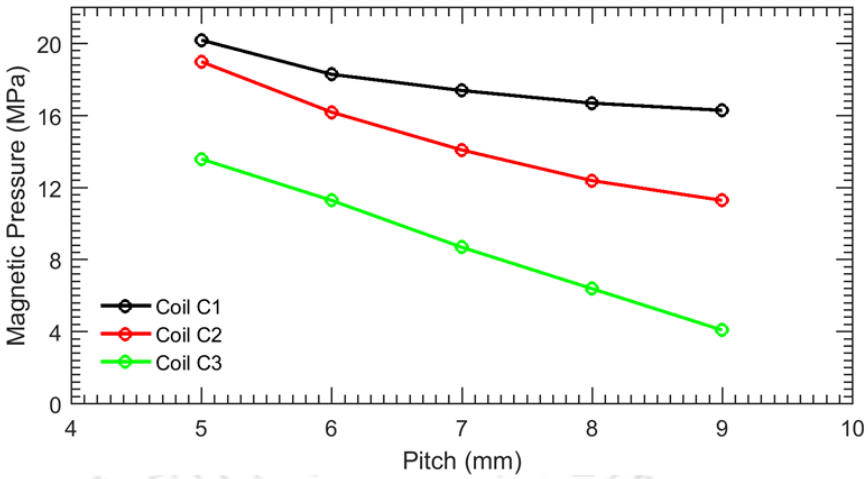

Figure 3.12: Effect of coil pitch on magnetic pressure

The simulated results show that for the coil C1 (relative size less than 1), the magnetic pressure distribution is non-uniform along the length with the maximum at centre of the tube. For coil C2 (relative size equal to 1), the magnetic pressure distribution is quite uniform along the axis of the tube. In case of coil C3 (relative size greater than 1), the magnetic pressure distribution becomes non-uniform with maximum at the tube ends. The results shows that as the relative size increases the magnetic pressure increases and becomes uniform as the value relative size approaches one. As the relative size is increased, the magnetic pressure distribution becomes non-uniform with higher magnetic pressure at the ends of the tube. The non-uniform distribution of the magnetic pressure is due to relative size of the tube-coil system. If the coil length is smaller than the tube length, the magnetic pressure is confined to a region smaller than the tube length and results in non-uniform distribution of magnetic pressure. The similar observation is obtained in case of coil length greater and equal to the tube length. As the relative size is increased, the frequency increases leading to increase in the skin depth. As the skin depth increases, the amount of the magnetic field retained inside the tube decreases and so, the magnetic pressure decreases as the coil length is increased. Figure 3.12 shows the effect of pitch on magnetic pressure during electromagnetic tube expansion. The pitch of coil was varied from 5 to 9 mm. For coil C1, the magnetic pressure decreases gradually from 20.2 MPa to 16.3 MPa. For coil C2, the magnetic pressure decreases from 18.9 MPa to 11.3 MPa. And for coil C3, the magnetic pressure decreases from 13.4 MPa to 4 MPa as the pitch of the coil is increased.

Table 3.3: Parameters to study the effect of current frequency

Voltage (kV)	0.24	1.22	2.45	3.67	4.9	6.12	7.34	8.57	9.79
Capacitance (μF)	37958	1518	379	168.7	94.9	60.73	42.18	30.99	23.72
Frequency (kHz)	1	5	10	15	20	25	30	35	40
Skin depth (mm)	2.59	1.16	0.82	0.67	0.58	0.52	0.47	0.44	0.41

3.4.2 Effect of Current Frequency

To study the effect of current frequency on electromagnetic tube expansion the discharge energy is kept constant at 1 kJ. Capacitance for each simulation is varied to get the frequency from 1 to 40 kHz at the interval of 5 kHz. The parameters, used for studying the influence of frequency during electromagnetic tube expansion of thicknesses from 0.4 to 1 mm with the interval of 0.2 mm, are tabulated in Table 3.3.

The effect of current frequency on the waveform of coil current is shown in Figure 3.13. It shows that as the frequency of coil current increases, the amplitude of current waveform increases while its period decreases, which is in good agreement with the theory of electromagnetism.

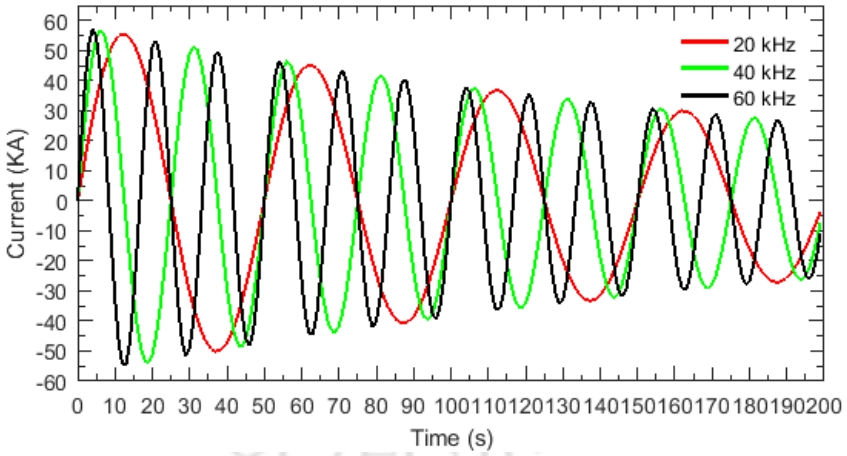

Figure 3.13: Current curves obtained at various frequencies

Effect of frequency on EM expansion of tube is studied by plotting the displacement at the midpoint along the tube's length for different thicknesses. Figure 3.14 shows that increase in the frequency increases the deformation because at low frequency as most of the magnetic flux leaks out of the tube due to larger skin depth. As frequency increases skin depth decreases and so magnetic flux leakage also decreases which increases of deformation. When the deformation reaches to the maximum for a particular frequency, then it starts decreasing with further

increase in frequency. The deformation increases rapidly up to 10 kHz, after that deformation increases slowly and attains its maximum value which can be explained using Figure 3.15. It shows that the value of skin depth decreases rapidly with increase in frequency up to 10 kHz and above 10 kHz it decreases gradually and tends to become constant with further increase in frequency.

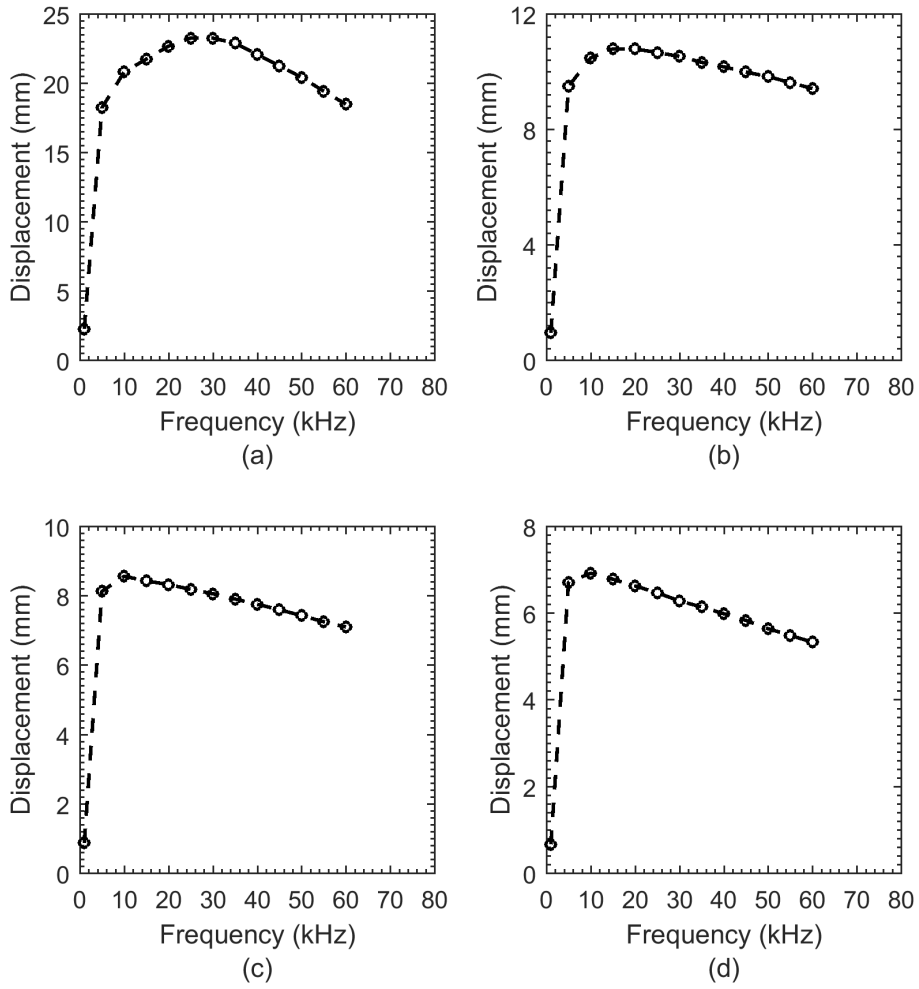

Figure 3.14: Effect of frequency on displacement for tube thickness of (a) 0.4 mm (b) 0.6 mm (c) 0.8 mm (d) 1 mm

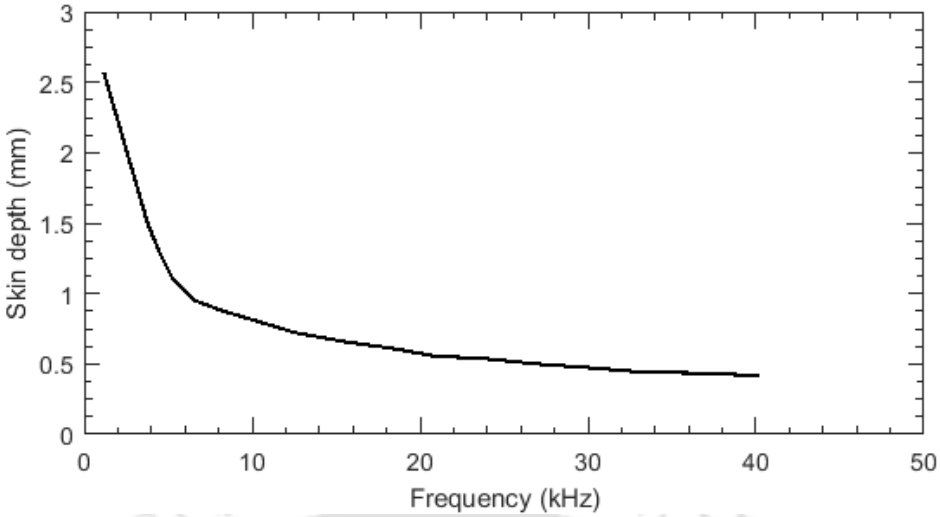

Figure 3.15: Variation of skin depth with frequency

After the displacement attains the maximum value corresponds to a frequency which depends on the thickness, the displacement starts decreasing slowly which can be explained by Figure 3.16, which shows that the eddy current phase lag increases with thickness.

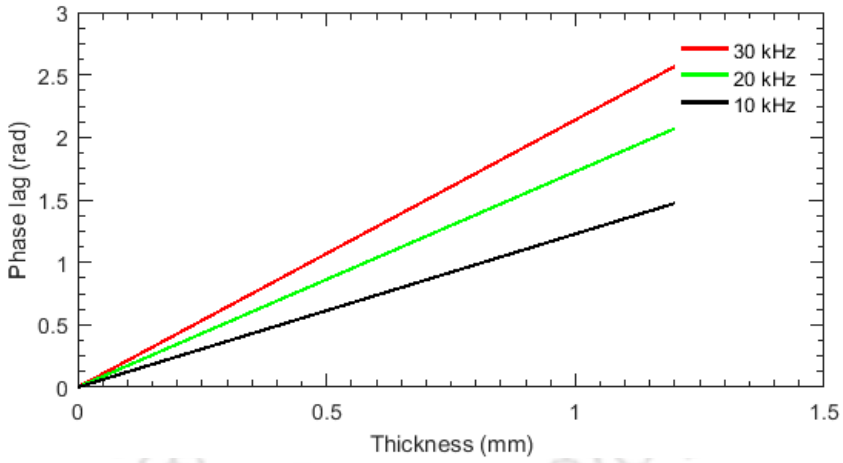

Figure 3.16: Eddy current phase lag

Figure 3.16 shows that the eddy current becomes out of phase which increases as we move through the thickness and results in to decrease in deformation as the frequency increases. The phase lag (θ) is the phase lag between the surface eddy current and the eddy current at certain depth as we move through the thickness of the tube as shown in Figure 3.17. The phase lag (θ) of the eddy current with depth (x) for a skin depth (δ) is given by [53]

$$\theta = \frac{x}{\delta} \tag{3.15}$$

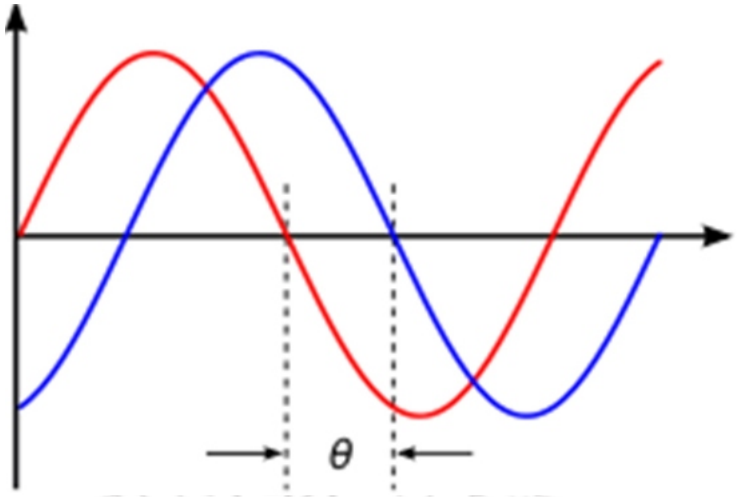

Figure 3.17: Phase lag between coil current and workpiece current

Figure 3.14 also shows that the deformation increases as the θ becomes equal to 1 and then it starts decreasing as θ increases beyond 1. Therefore for optimum deformation, the value of θ has to be nearly equal to 1. Figure 3.18 shows the effect of frequency on electromagnetic expansion of tube for different thickness of tube. It shows that as the frequency increases, displacement also increases and achieves maximum displacement at the optimum frequency which depends upon the thickness of the tube. It also shows the effect of frequency on the deformation is more prominent for thinner tubes. The optimum frequency is found to be in the range of 10-30 kHz for the simulated system for 0.4 to 0.8 mm thick tubes. Table 3.4 shows the optimum frequency for various thickness of tube. It shows that the optimum skin depth varies from 0.92 t0 1.125 of the thickness of tube.

Table 3.4: Optimum frequency for various thickness of tube

Thickness (mm)	Optimum Frequency (kHz)	Skin Depth (mm)	Skin Depth as % of Thickness
0.4	26	0.50	1.25
0.6	16	0.59	0.98
0.8	10.8	0.76	0.95
1	9.9	0.92	0.92

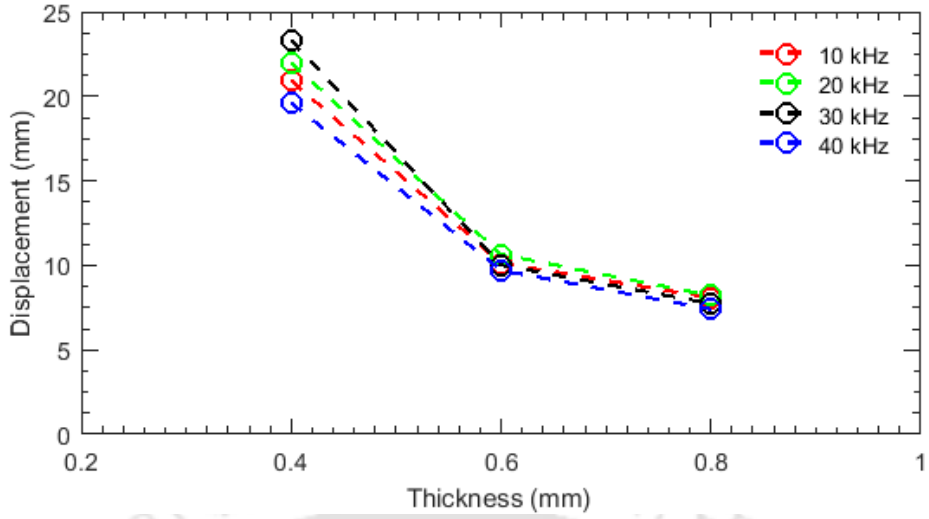

Figure 3.18: Variation of displacement with current frequency and thickness of tube

3.4.3 Formability Analysis

Forming limit defines the local thinning of the material during forming, which leads to failure. The most common way to represent the forming limit is the forming limit diagram. A forming limit diagram is used to determine the forming behaviour of a material. The forming limit separates the safe region from failure region on a major-minor strain plot. The method involves the marking of material surface with circular marks before forming and then measuring the axes of ellipse after deformation to plot the forming limit curve. In this case, the tubes were marked with circular marks as shown in Figure 3.19.

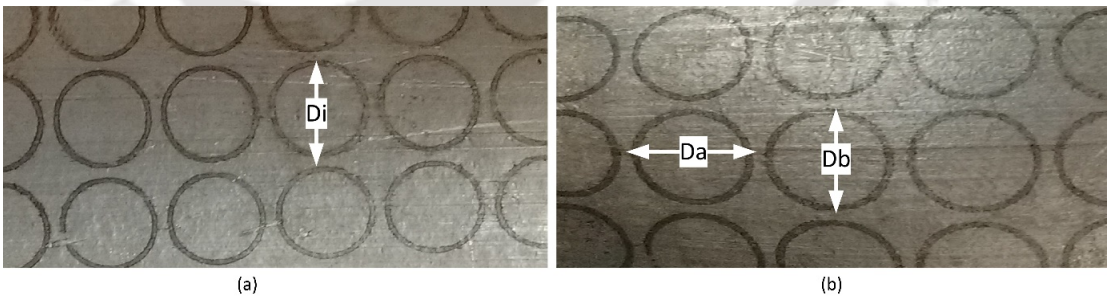

Figure 3.19: Circular marks on tube surface (a) before forming (b) after forming

The tubes were electromagnetically deformed and the axes of ellipse were measured to get the safe and unsafe strain values. For coil-tube length ratio equal to 1, the electromagnetic forming results into tearing at edges. The tube was uniformly deformed as the tube and coil were of the same length, resulting in uniform pressure. The axes of the deformed circles were measured to get the strain values using Eq. (3.16) and (3.17).

$$\text{Major strain} = \frac{\text{Major axis length}\,(D_a) - \text{Initial circle diameter}\,(D_i)}{\text{Initial circle diameter}\,(D_i)} \tag{3.16}$$

$$\text{Minor strain} = \frac{\text{Minor axis length}(D_b) - \text{Initial circle diameter}(D_i)}{\text{Initial circle diameter}(D_i)} \tag{3.17}$$

The strain values were measured at two regions as near the tube failure and away from the tube failure region. The strain values at points near the tube failure are considered as unsafe while strain values at points away from the failure are considered safe. Figure 3.20. shows the strain values distinguishing the safe and unsafe region for the coil-tube ratio equal to one. The strain values fall in the uniaxial region of forming limit curve.

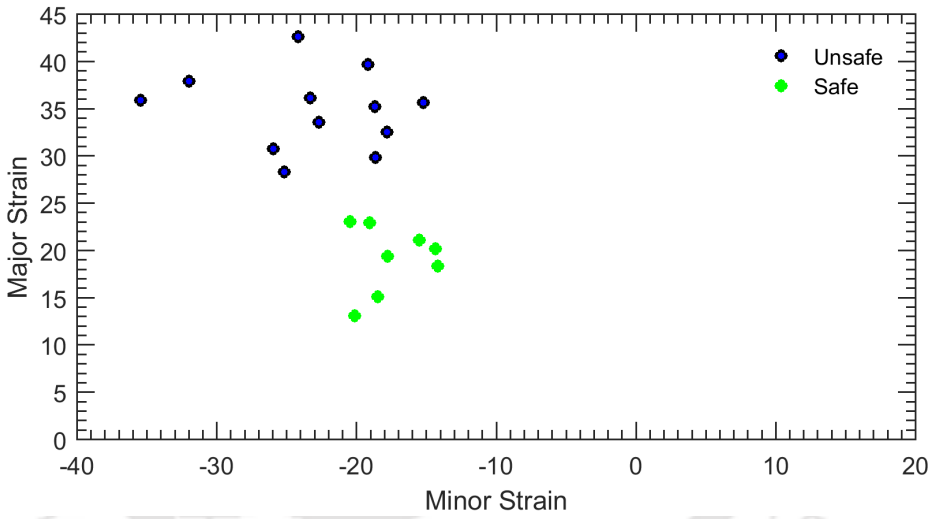

Figure 3.20: Strain values for coil-tube length ratio equal to one

For coil-tube length ratio less than one, electromagnetic tube forming results into failure at the centre of the tube. As the coil is shorter than the tube length, the bulging is confined to the central region of tube. The deformed circle diameters were measured to find out the minor and major strains. The strain values obtained for the coil-tube length ratio less than one are shown in Figure 3.21. The strain values are confined to the biaxial region of the forming limit curve.

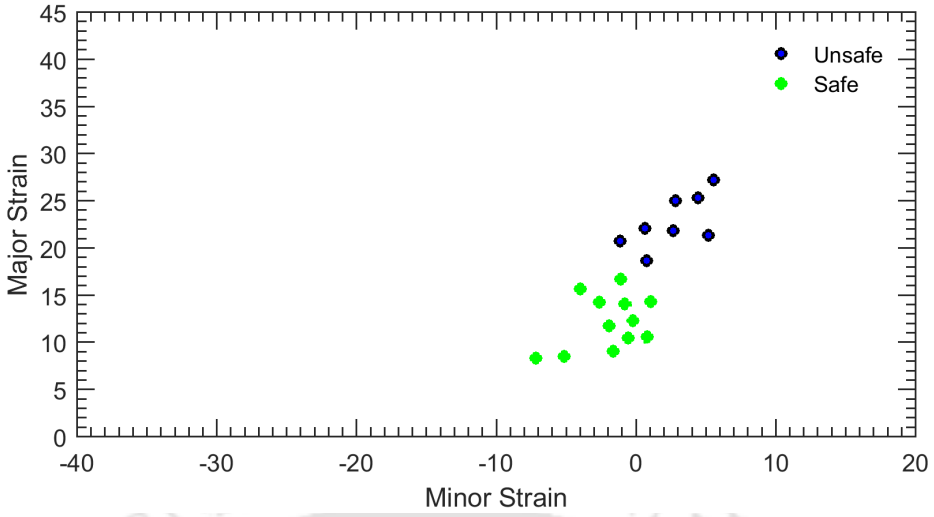

Figure 3.21: Strain values for coil-tube length ratio smaller than one

For the coil-tube length ratio more than one, the failure takes place at tube edge as shown in Figure 3.22. As the coil length was more than the tube length, non-uniform deformation leads to flanging of the tube. The deformed circle diameters were recorded to calculate the strain and the strain values which were plotted as shown in Figure 3.23. The strain values fall in the uniaxial region of forming limit curve.

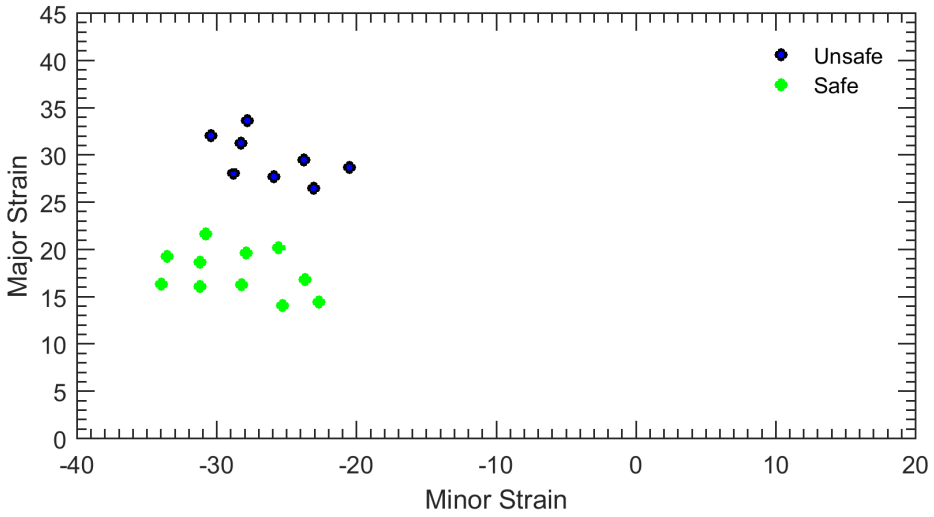

Figure 3.22: Strain values for coil-tube length ratio greater than one

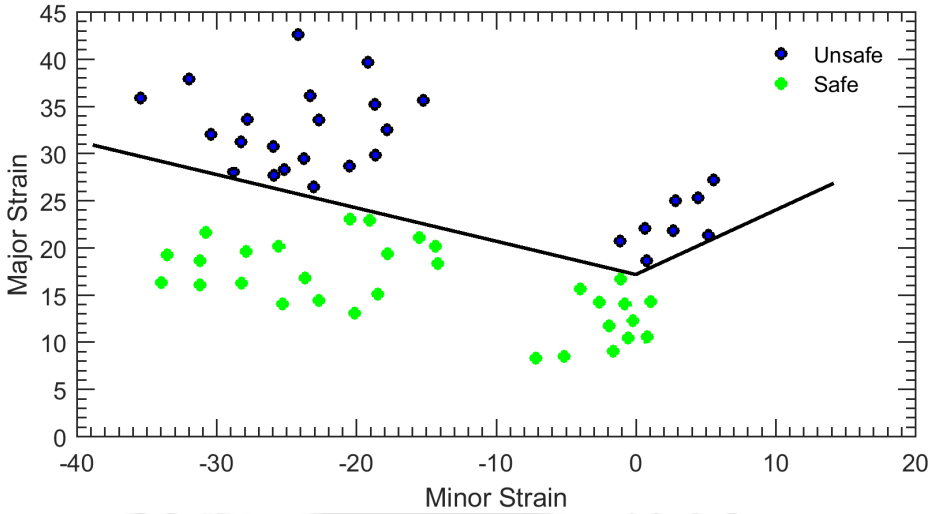

Figure 3.23: Forming limit diagram of AA 6061

3.5 Summary

1. The electromagnetic tube experiments were carried out to study the effect of coil-tube relative length. The simulated results were found to be in good agreement with an error of about 6.4 %.

2. The coil current amplitude and current frequency decrease with the increase of coil length. The maximum currents for coils C1, C2 and C3 are 112 kA, 92 kA and 82 kA, respectively at 5.3 kJ discharge energy.

3. When the coil length is smaller than the tube length, tube deformation is non-uniform along the length, and deformation at tube centre is more than at tube ends. When the coil length is equal to the tube length, the tube deformation along the length is uniform. When the coil length is greater than tube length, the tube deformation is non-uniform along the length, and deformation at tube ends is more than at the tube centre.

4. The maximum magnetic pressure decreases with the increase in coil length and pitch i.e. magnetic pressure is inversely proportional to the coil length and pitch. The maximum magnetic pressure obtained for the coils C1, C2 and C3 are 20.2 MPa, 18.9 MPa and 13.4 MPa, respectively, at 5.3 kJ discharge energy.

5. When the coil length is smaller than the tube length, the magnetic pressure is greater at the centre. When the coil length is equal to the tube length, the magnetic pressure is uniform. For the coil length greater than the tube length, the magnetic pressure is more at the tube ends.

6. The distribution of the magnetic pressure can be changed by varying the coil-tube relative length, which can be used to manufacture different products. For example, shorter length coil for welding, equal length coil for cladding and longer length coil for flanging.

7. The effect of current frequency on electromagnetic tube expansion is analyzed using finite element simulation. The results show that as the frequency increases, deformation increases due to the decrease of the skin depth. As the frequency is increased beyond the optimum value, the tube deformation decreases due to induced current become out of phase as we move through the tube thickness. As the frequency increases, the phase angle between the eddy current and input current increases which results into decrease in tube deformation.

8. The optimum frequency in the presented analysis corresponds to the maximum displacement. Effect of frequency on deformation is more prominent for thin tubes.Therefore, the effect of frequency can be neglected for thick tubes provided available magnetic pressure can deform the tube. The boundary between the thin and thick tubes is decided by the skin depth with respect to frequency plot of that material. For the simulated system, the optimum frequency range is found to be 10 kHz to 30 kHz for the AA 6061 alloy with thickness varied from 0.4 to 1 mm.

CHAPTER 4

Electromagnetic Sheet Forming

4.1 Dual Electromagnetic Sheet Forming

Energy efficiency of the dual electromagnetic forming is compared with the single-sided electromagnetic forming using FEM simulations. For rectangular coil generating uniform pressure, the top layer of the coil assists in the deformation of the workpiece while the bottom layer hinders the workpiece deformation. To make the bottom layer of the coil also to assist in the deformation of the workpiece, a uniform pressure rectangular coil is designed and placed between the two sheet metal workpieces. The efficiencies of the two processes are compared in terms of the maximum deformation obtained for each case.

In the present study, a dual electromagnetic sheet metal forming is proposed to improve the efficiency of electromagnetic sheet metal forming using a uniform pressure coil. Use of uniform pressure actuator to form two sheets can increase the productivity. Dual electromagnetic forming can be used to form parts like petrol tank. Finite element analysis is performed to compare the single sheet electromagnetic forming and the dual sheet electromagnetic forming on the basis of the final deformation.

4.1.1 Finite Element Modelling of Electromagnetic Forming

Electromagnetic sheet forming simulations are carried out using a uniform pressure coil. In the present work, dual electromagnetic forming of the sheet is analyzed using finite element simulations in LS-DYNA. By carrying out simulations, the comparison is made between the electromagnetic forming of the single sheet and two sheets using the uniform pressure coil. To simulate the electromagnetic sheet forming, a combination of Finite Element Method for conductor parts and Boundary Element Method for the surrounding air is implemented using the finite element code LS-DYNA. The boundary element represents the boundary of the

conductor and air. The air was not meshed in the simulation and the current profiles are directly mapped from coil to the tube using boundary element method. The use of the BEM for the air allows to handle complex 3D geometries with multiply connected conductors and motion of the conductors. The variable of the BEM is a surface current allowing the connection of the model to external current sources by simple Dirichlet constraints. The material property of Al6061 is listed in Table 4.1. The rate-dependent material model is used to study the deformation of the workpiece. The coil is considered to be rigid for simulation. The R-L-C parameters used are the resistance of 10.5 mΩ, the inductance of 359 mH and the capacitance of 426 µF.

Table 4.1: AA 6061 material constants

Density (ρ)	2700 kg/m^3
Modulus of rigidity (G)	26 GPa
Modulus of Elasticity (E)	68.9 GPa
Poisson's Ratio (γ)	0.33
Electrical Conductivity (σ)	25 MS/m

Figure 4.1 shows dimensions of the coil and the sheet system used for the simulations. The coil has 12 turns, pitch 8 mm with the cross-section of 5×6 mm^2. The workpiece is of size 92×70 mm^2 with 1 mm thickness. The standoff distance between the coil and the workpiece is 0.5 mm.

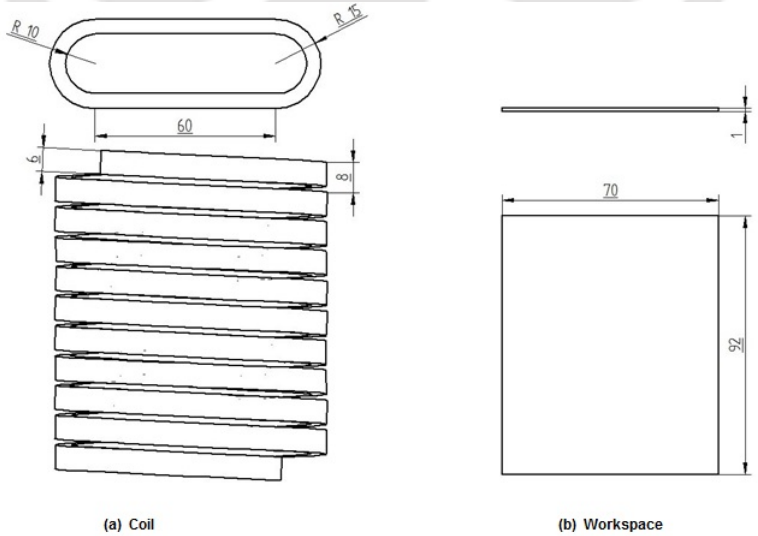

Figure 4.1: Dimensions of coil and workpiece

The meshed finite element coil and workpiece are shown in Figure 4.1. Both coil

and workpiece are meshed using hexahedral solid elements.

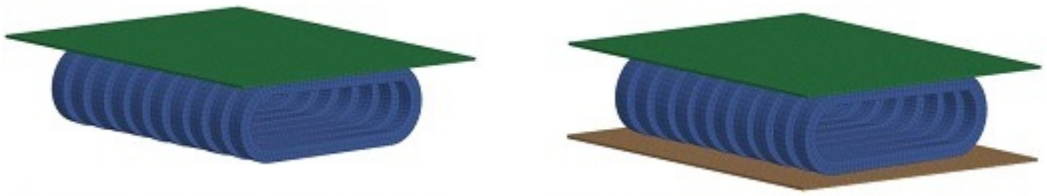

Figure 4.2: Meshed coil and workpiece

4.1.2 Results and Discussion

The finite element electromagnetic forming simulations of a single sheet and dual sheet configurations are carried out at different voltages (2 kV, 3 kV, 4 kV, 5 kV). Figure 4.3 shows the deformed profile of the workpiece.

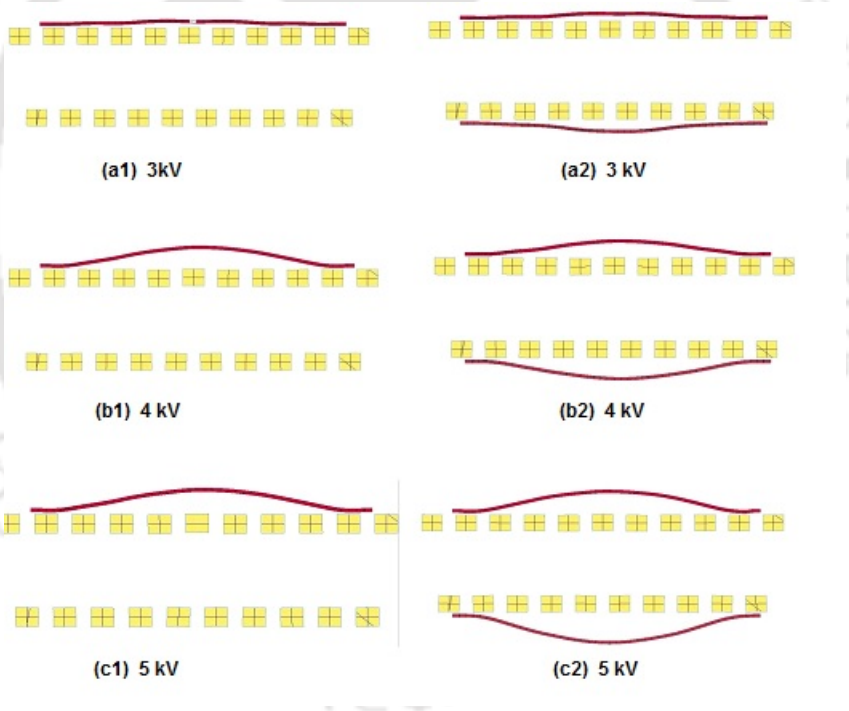

Figure 4.3: Deformed profile of workpiece

It shows that for the same voltage, deformation obtained in the case of the dual sheet is equal to or higher than that of single sheet electromagnetic forming. The lesser deformation obtained in case of the single sheet forming is due to the opposing nature of the current flowing through the bottom layer of the coil. In case of the uniform pressure coil, the top layer of the coil assists the deformation of the workpiece while the bottom layer restricts the deformation. The bottom layer of the coil opposes the deformation of the workpiece because the current flowing

through the bottom layer is in opposite direction as that of the top layer of the coil. The opposing nature of the currents in the bottom layer can be explained by plotting maximum current density in the coil for the single sheet and the dual sheet electromagnetic forming as shown in Figure 4.4.

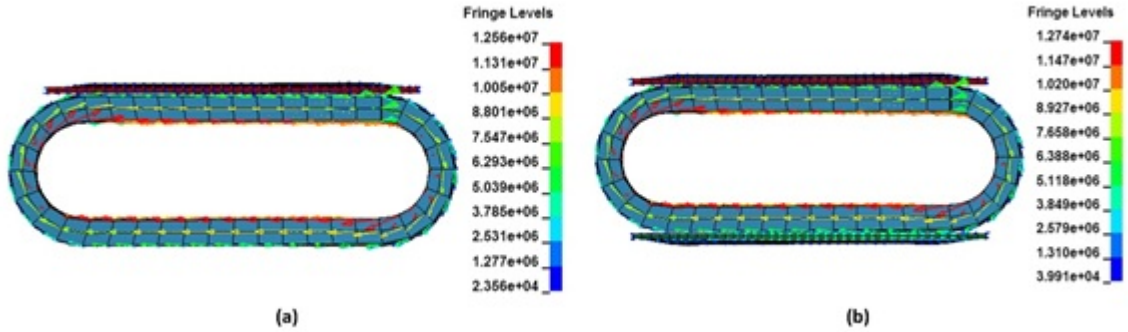

Figure 4.4: Current density in the coil (a) Single sheet (b) Dual sheet

Figure 4.4 shows that the current flowing in the coil's bottom layer is in the opposite direction as that of the coil's top layer. The direction of current flowing in the sheet depends on whether the sheet is placed near to the top layer or bottom layer of the coil. The direction of current in the sheet is in the opposite direction as that of current direction in the layer, near to which the sheet is placed. Now, according to the Bio-Savart law, two current carrying conductors attract each other when the current is in the same direction and repel each other when the current is in the opposite direction. Therefore, in case of the single sheet forming, the bottom layer of the coil hinders the deformation of the workpiece. In case of the dual sheet forming, the presence of the bottom sheet confines the magnetic field in between the bottom sheet and bottom layer of the coil and therefore, the deformation obtained in case of the dual sheet forming is equal to or more than that of single sheet forming. Figure 4.4 also shows that the current density obtained in case of the dual sheet forming is more than that of the single sheet forming. Figure 4.5 shows the Lorentz force in case of the single and the dual sheet forming.

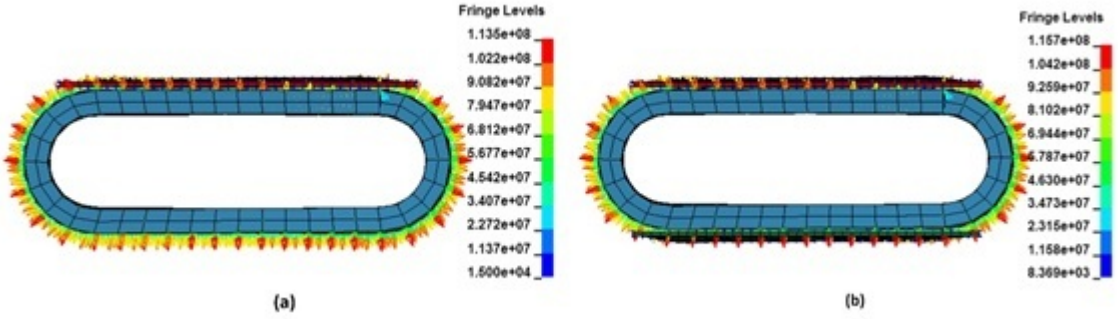

Figure 4.5: Lorentz force distribution $(\mathrm{N/m^3})(a)Singlesheet(b)Dualsheet$

The Lorentz force obtained in case of the dual sheet forming is more than that of the single sheet forming. The elimination of the opposing nature of the bottom layer results into increase in the deformation of the workpiece in the case of the dual electromagnetic forming of the sheet. Figure 4.6 shows the corresponding deformation of the central portion of the sheet.

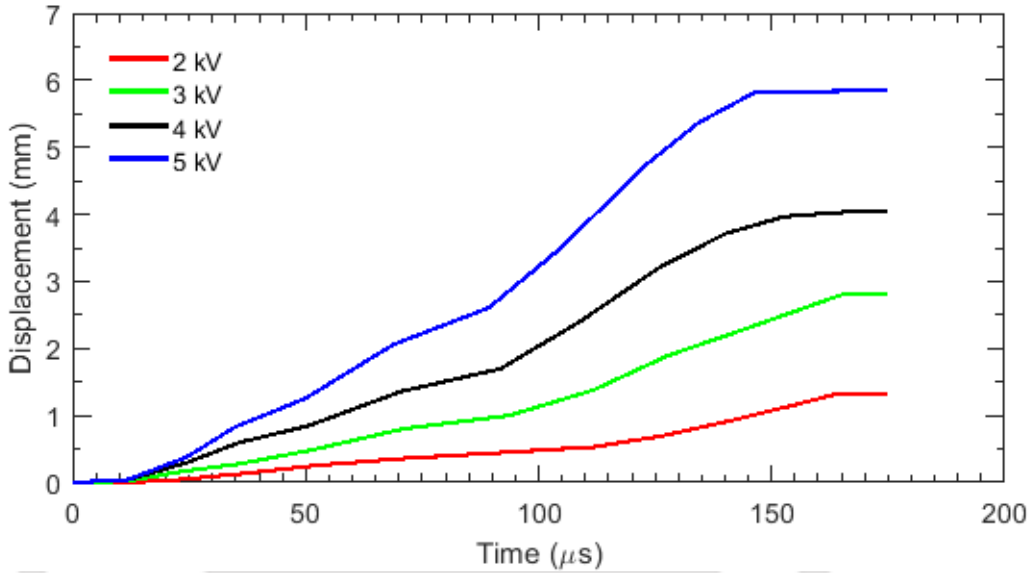

Figure 4.6: Deformatin of single sheet electromagnetic forming with respect to time

The deformation of the workpiece increases as the voltage is increased with maximum deformation obtained at 5 kV is 5.8 mm. Figure 4.7 shows the deformation of the central portion of the sheet in the dual sheet electromagnetic forming case. The deformation of the workpiece increases as the voltage is increased with maximum deformation obtained at 5 kV as 6.5 mm.

Figure 4.8 shows the comparison of the deformation obtained by the single sheet electromagnetic forming and dual sheet electromagnetic forming using uniform pressure coil at various voltages. The deformation obtained in the case of the dual sheet electromagnetic forming is equal or higher than that of the single sheet electromagnetic forming. By placing the bottom sheet, the mutual inductance between the bottom layer of the coil and the bottom workpiece increases, which results in the increase in deformation in case of dual electromagnetic forming. The deformation difference between the two cases increases as the voltage is increased due to an increase in the opposing force of the bottom layer with the voltage.

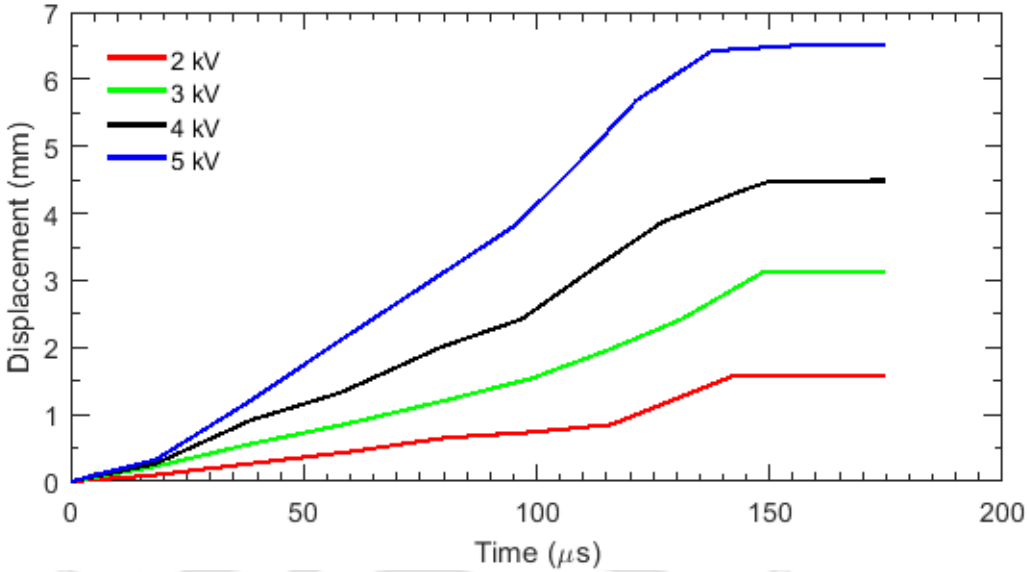

Figure 4.7: Deformatin of dual sheet electromagnetic forming with respect to time

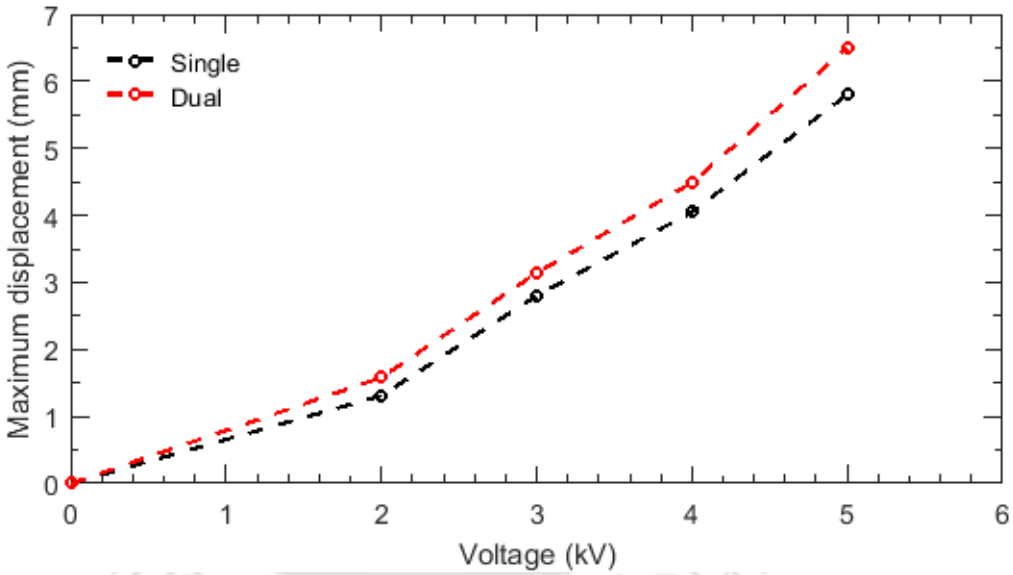

Figure 4.8: Comparision of single sheet and dual sheet electromagnetic forming

4.2 Crow-barring effect during Electromagnetic Sheet Forming

The experimental setup consists of a capacitor bank, a spiral coil, and a die. The circuit diagram with the experimental setup is shown in Figure 4.9.

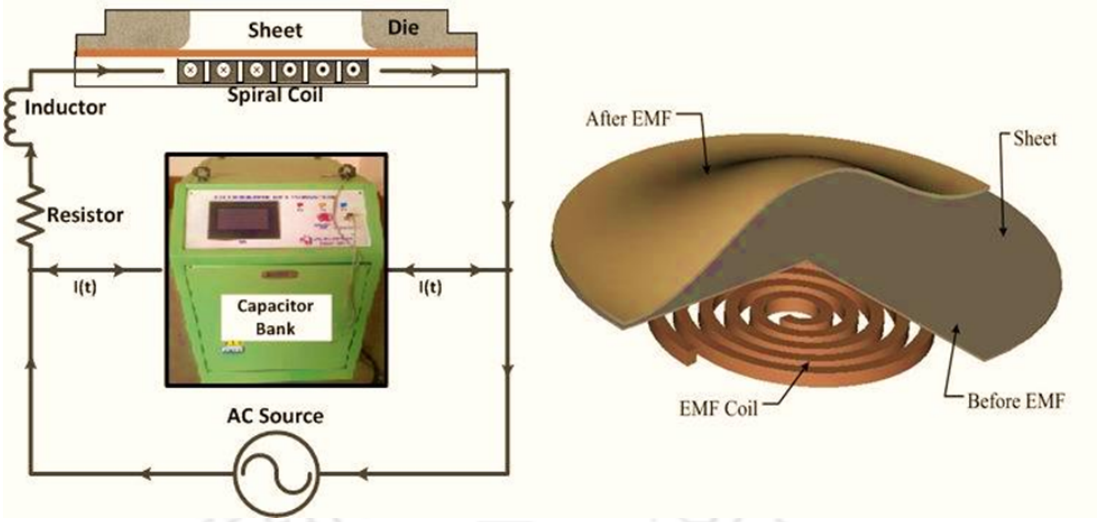

Figure 4.9: Setup for electromagnetic sheet forming

Takatsu et al. [37] carried out the electromagnetic forming on a circular flat sheet of annealed AA 1050 alloy of 110 mm diameter with 0.5 mm thickness. The blank holder was having an internal diameter of 80 mm. The spiral coil used for deformation had 5 turns with an effective diameter of 80 mm and 5.5 mm pitch. Takatsu et al. carried out their experiments with the flat spiral coil connected to the electromagnetic circuit having the capacitance of 40 µF, total inductance of 2.86 µH and resistance of 28.5 mΩ with the capacitor bank energy of 6 kV. The gap between the coil and the workpiece was equal to 1.6 mm.

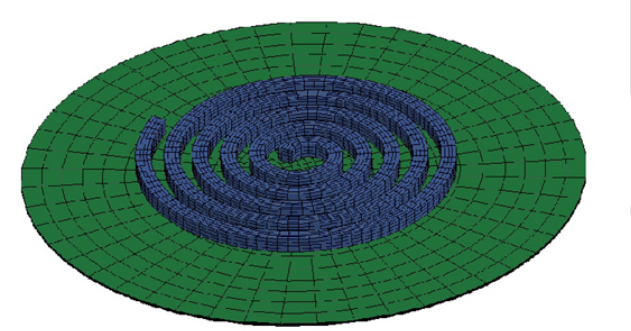

Figure 4.10: Meshed coil and workpiece

During simulations, the sheet was modelled as a deformable body and meshed with reduced integration hexagonal elements. The thickness of the workpiece had 3 elements while the surface was modelled with 1523 elements. The holder and the coil were modelled as rigid bodies. The contact between sheet and holder was taken as the surface to surface contact with the coefficient of friction equal to 0.25. Figure 4.10 shows the meshed coil and workpiece used for the simulation. The geometry details, material and electrical properties of coil used for finite element simulation are tabulated in Table 4.2.

Table 4.2: Coil geometrical parameters with material constants

No of windings	5
Material	Copper
Maximum diameter of spiral coil	80 mm
Pitch	5.5 mm
Circuit Capacitance	40 µF
Electrical conductivity	58 MS/m

The material constants of workpiece used for finite element simulation are tabulated in Table 4.3.

Table 4.3: AA 1050 material constants

Thickness	0.5 mm
Diameter	110 mm
Electrical conductivity	36 MS/m
Density	2750 kg/m^3
Young's modulus	80.7 GPa
Poisson's ratio	0.33

The aluminium sheet was considered to be isotropic. Rate-dependent Hollomon law was used for modelling the high strain rate EMF process as

$$\sigma_y = \sigma_0 \varepsilon^n D \dot{\varepsilon}^m \tag{4.1}$$

where σ_y is the effective stress, ε^p is the effective plastic strain, $\dot{\varepsilon^p}$ is the effective plastic strain rate, σ_0 material constant, n is the hardening exponent, and m and D are the rate dependent exponent and multiplying factor respectively. The value of n was equal to 0.27 and the material constant equal to 118 MPa. These values were used from the published literature of Takatsu et al. [37]. Values of exponent m and D used were considered equal to 0.075 and 1.7 respectively. So Eq. (4.2) can be simplified for the used AA 1050 material as

$$\sigma_y = 201 \varepsilon^{0.27} \dot{\varepsilon}^{0.075} \tag{4.2}$$

Figure 4.11 show the stress-strain relationship used for the simulation of electromagnetic sheet metal forming.

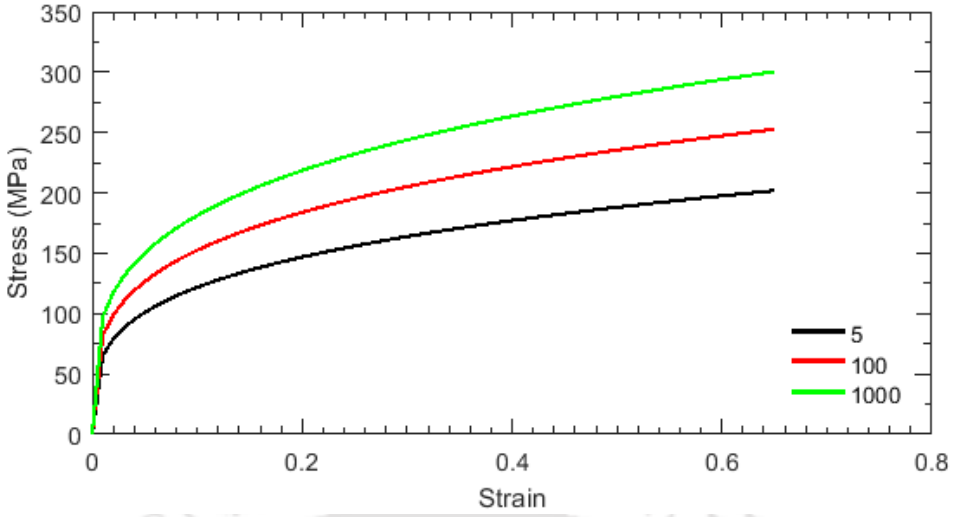

Figure 4.11: Stress-strain curve at various strain rates

To validate the finite element model of electromagnetic sheet metal forming experimental results from Takatsu et al. [49] was taken as a reference. Figure 4.12 and Figure 4.13 show the comparison between the simulated and measured vertical deflection at centre and 20 mm away from centre.

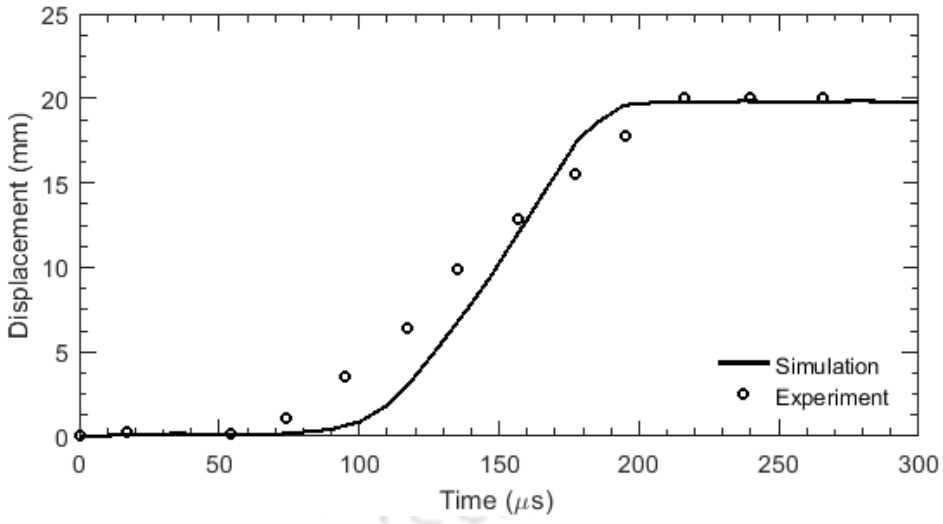

Figure 4.12: Measured and simulated vertical displacement at centre

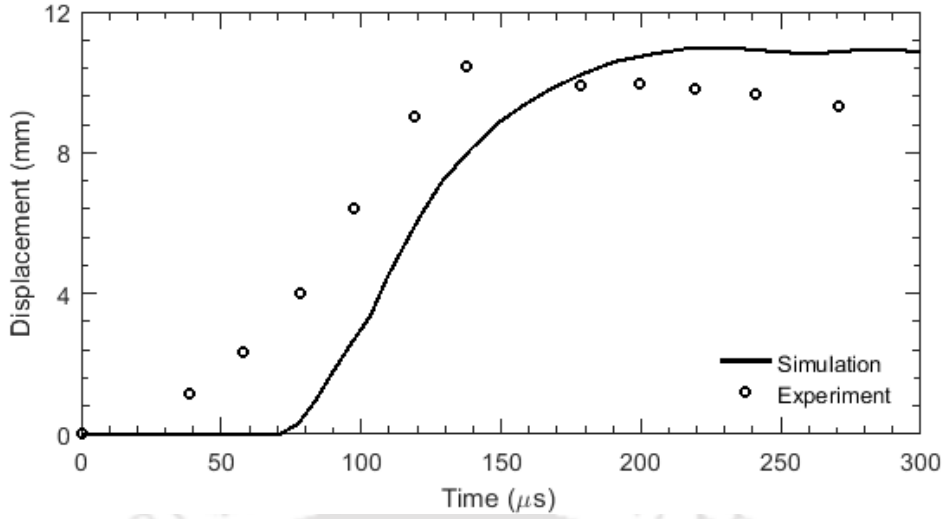

Figure 4.13: Measured and simulated vertical displacement at 20 mm from center

In Figure 4.12 and Figure 4.13, the solid lines represent the simulation results while the circles represent the experimental results obtained by Takatsu et al. [49]. The simulated results for vertical displacement with respect to time are in good agreement with experimental results. In the simulation, the mesh size of the sheet increases as one moves away from the center of the sheet. Therefore, the simulation results for point 20 mm away from the center of the sheet are not in match with the experimental results as compared to the centre of the sheet. The simulation results can be further refined by using fine meshing for the sheet but due to the limitation of computation capacity, further refinement was not considered. Figure 4.14 shows the deformed mesh of the workpiece at different time intervals. The sheet got deformed at the periphery and not at the centre during 90 µs. A significant increase in deformation was observed at 150 µs, 180 µs and 210 µs at the point away from centre.

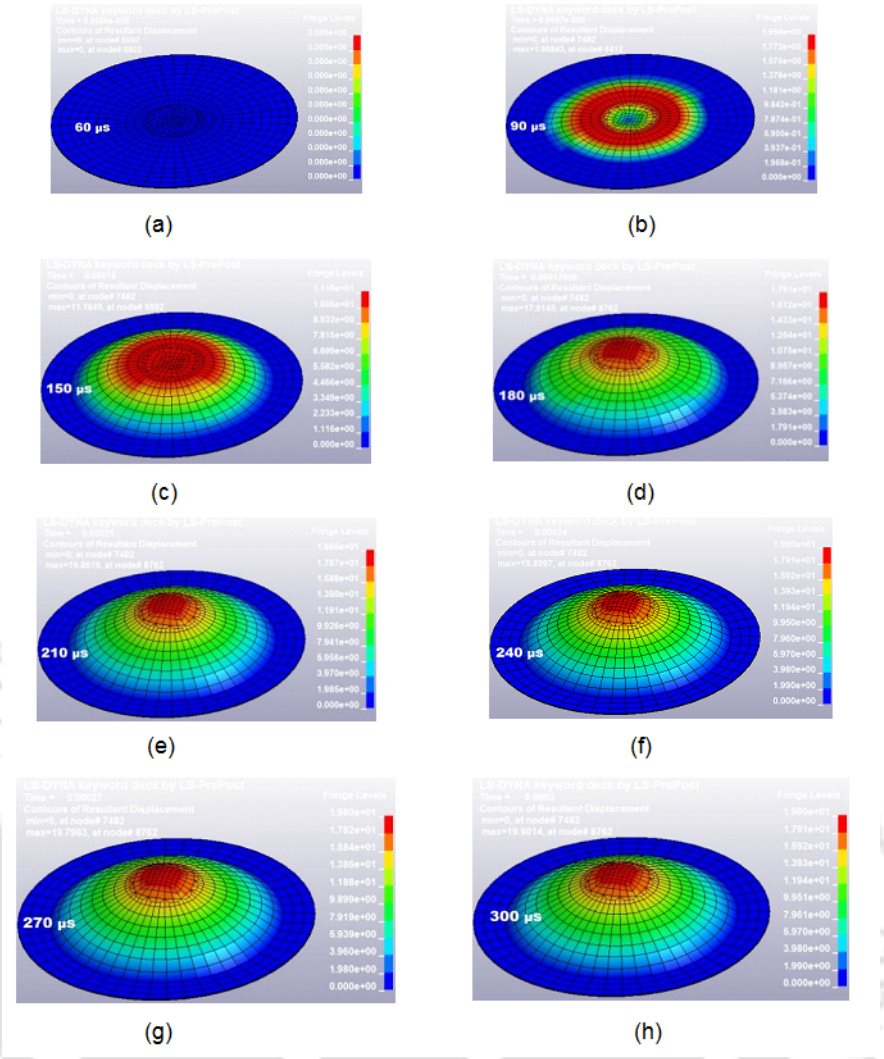

Figure 4.14: Simulated geometry of the sheet at (a) 19 µs (b) 90 µs (c) 150 µs (d) 180 µs (e) 210 µs (f) 240 µs (g) 270 µs (h) 300 µs

In case of the spiral coil magnetic field at the centre of the coil is less at the periphery of the coil. Due to this reason, sheets did not deform at the centre as the dead zone of the spiral coil was formed at the centre. Subsequently, at 180 µs, the central part of the sheet started bulging and maximum bulge height of 19 mm was achieved at 240 µs. Further increase in time to 270 µs and 300 µs did not lead to significant increase in deformation. The deformed meshes obtained from the simulation were found qualitatively in agreement with the high-speed photographs of the workpiece obtained by Takatsu et al. [49]. It was clear from Figure 4.14 that the centre part of the workpiece remained at rest initially due to negligible magnetic pressure developed in that region while the maximum magnetic pressure occurred at about 20 mm away from the centre. Due to this type of uneven magnetic pressure, local thinning occurred which can be overcome by using coils that produce more uniform magnetic field. Figure 4.15 shows the deformation profiles of the workpiece obtained from FE simulation at different time intervals.

It is evident from the Figure 4.15 that at 75 and 95 microseconds the sheet did not deform significantly at the centre. The magnetic pressure obtained at the centre was almost zero initially and it was maximum at about 20 mm radius. The deformation profiles of the workpiece shown in Figure 4.15 are in good agreement with the experimental results reported in the literature by Takatsu et al. [49].

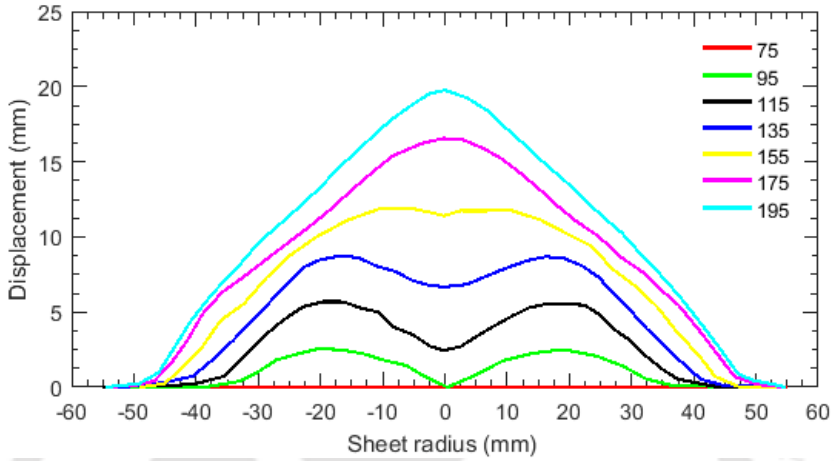

Figure 4.15: Deformation profiles of the workpiece with time

The crow-barring of the current pulse can be implemented either by diverting the ineffective current pulses to some other storage unit or by installing high-power diodes in parallel with the capacitor, which can automatically turn on the crowbar circuit upon voltage reversal [54].To study the effect of crow-barring the current pulse on the workpiece deformation during electromagnetic sheet metal forming, current supply was provided for a part of the cycle time during simulation and the corresponding sheet deformation was studied. Figure 4.16 and Figure 4.18 shows that as the number of the current cycle used for the simulation increases the displacement also increases at centre and at 20 mm radius. But after 1.5 current cycles the displacement remains constant. It means that the current pulses after the second current cycle are not contributing to the deformation of the sheet. In the present simulation, only one and half part of the current pulse was found to be responsible for the deformation.

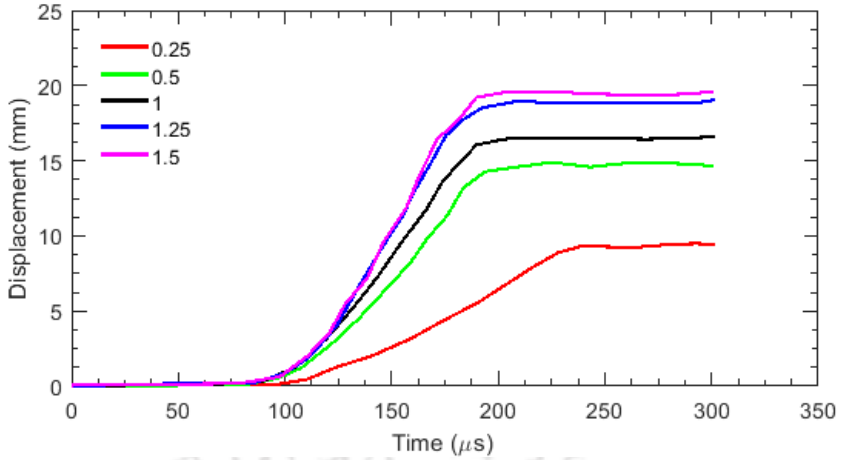

Figure 4.16: Effect of crow-barring at centre of the sheet

Figure 4.16 shows the deformation at the centre of the workpiece using a portion of current pulse. The value 0.25, 0.5, 1, 1.25, 1.5 represents the one-fourth, half and one complete cycle of the current pulse. From Figure 4.16 it is clear that the maximum deformation occurs at 1.5 part of the current pulse which is equal to the deformation obtained without crow-barring. Therefore, it can be concluded that only 1.5 part of the current is responsible for the forming and rest of the pulses can be neglected. Figure 4.17 shows the current pulse without and with crow-barring for 1.5 cycles of the current pulse.

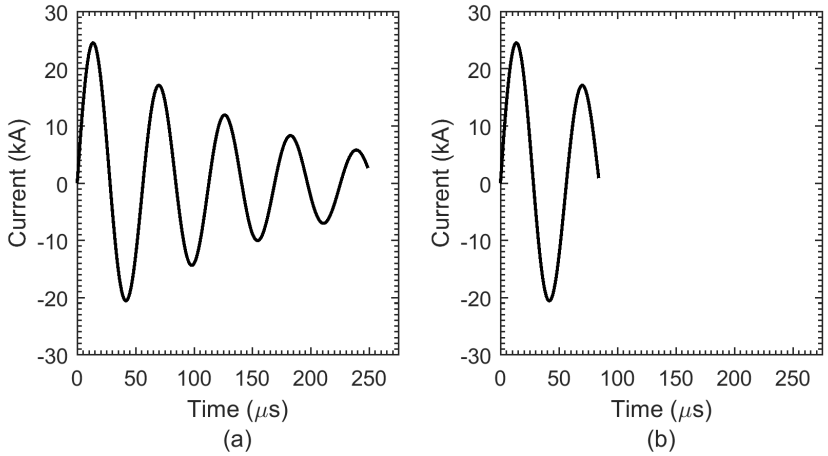

Figure 4.17: Current pulse (a) without crow-barring (b) with crow-barring

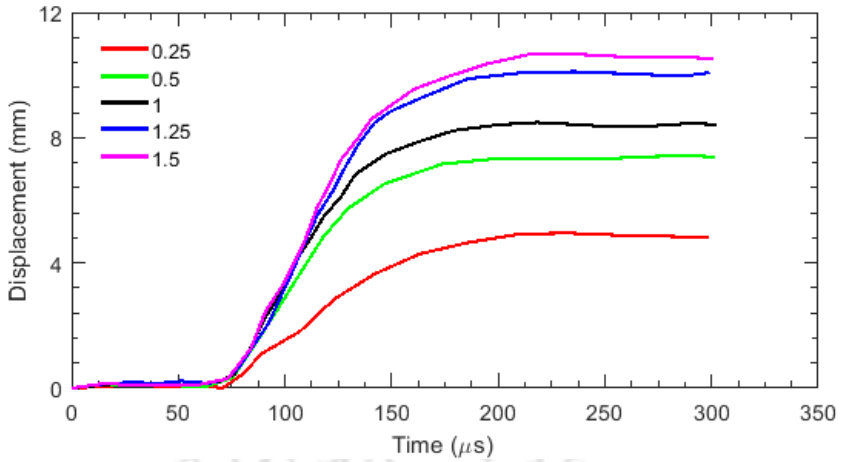

Figure 4.18: Effect of crow-barring at 20 mm from centre of the sheet

Figure 4.18 shows the deformation at 20 mm away from the centre of the work-piece using a portion of the current pulse. From Figure 4.18 it is clear that the maximum deformation occurs at 1.25 part of the current pulse which is equal to the deformation obtained without crow-barring. The difference in the portion of the current pulse responsible for maximum deformation in case of central region and at 20 mm away from the centre is due to the non-uniform deformation of the sheet, as the central portion of the sheet does not deform initially due to weak magnetic field in the central region.

4.3 Summary

1. Finite element simulations of electromagnetic single and dual sheet forming configurations are performed using a uniform pressure coil. The maximum deformation obtained in the case of single sheet electromagnetic forming is 5.8 mm at 5 kV while for the dual sheet electromagnetic forming is 6.5 mm at 5 kV. The lower value of deformation in the former case is due to the opposing nature of the magnetic field and forces created by the bottom layer of the coil. The increase in deformation in the latter case is more prominent as the voltage is increased due to increased opposing force of the bottom layer.

2. The finite element analysis of electromagnetic forming was carried out to study the effect of crow-barring of current pulse. The sinusoidal nature of the current pulse can result in reduced life of capacitor bank and at the same time only a part of the current pulse is responsible for forming. Therefore to know the part of the current pulse which is actually responsible for forming, the electromagnetic sheet metal forming simulations were carried out using crow-barred current pulses. The deformation obtained using crow-barred current pulses were compared with the

deformation obtained without crow-barring in FEA. Central part of the sheet did not deform initially due to dead zone at the centre and the maximum displacement obtained is 19 mm. It was found out that only first one and half cycles of the current pulse were responsible for the actual deformation and rest of the pulses can be crow-barred to increase the capacitor life and save the energy.

CHAPTER 5

Electromagnetic Forming and Perforation of Sheet

In this chapter, electromagnetic forming and perforation of the sheet is investigated. Electromagnetic forming and perforation is a novel method to carry out the simultaneous forming and perforation of the sheet. As no information regarding simultaneous forming and perforation of the sheet was found in literature, firstly a feasibility study was performed. The aim is to form a product shown in Figure 5.1

Figure 5.1: Washing machine component

The washing machine component shown in Figure 5.1 requires both forming and perforation operations to be performed. In conventional forming, both these operations are performed separately. Simultaneous forming and perforation of aluminium sheets can significantly increase the productivity. In the current research work, the feasibility study for simultaneous EM forming and perforation of sheets with detail analysis of the effect of process parameters has been carried out. Electromagnetic shearing is a recently developed non-conventional manufacturing process that can fulfill the increasing demands of the flexible manufacturing market. This process is carried out at a very high velocity of about 200 m/s and hence

called as high-speed shearing and can produce very complex shapes that are not possible with the conventional method. Since it is a single side shearing method, the requirement of matching the tooling set is eliminated which will reduce the production time. Clearance is a very crucial parameter during the shearing operation, a large clearance results in burr formation while a small clearance leads to burr-free surface but small clearance is difficult to obtain. Electromagnetic shearing has a number of advantages over the other methods like it can shear very thin materials with almost zero clearance angles and can cut the workpiece into any desired shape. Now since it is a high-velocity shearing, the waves created at this high velocity can completely change mechanics of the material near the cutting zone. Two types of die namely: negative and positive die were considered to perform the electromagnetic forming and perforation of sheets. Initially, feasibility test for perforation was conducted. In the first attempt, some nails were used as punch and experiments were performed at different discharge energies. It was found that 4.4 kJ discharge energy is sufficient to only perforate the AA 1050 of 1 mm thickness. After successful feasibility testing of perforation further study was carried out for the feasibility of simultaneous forming and perforation of AA 1050 sheets.

5.1 EMFP Die Design

The EMFP die used for experiments is shown in Figure 5.2. Two types of dies were used, negative and positive.

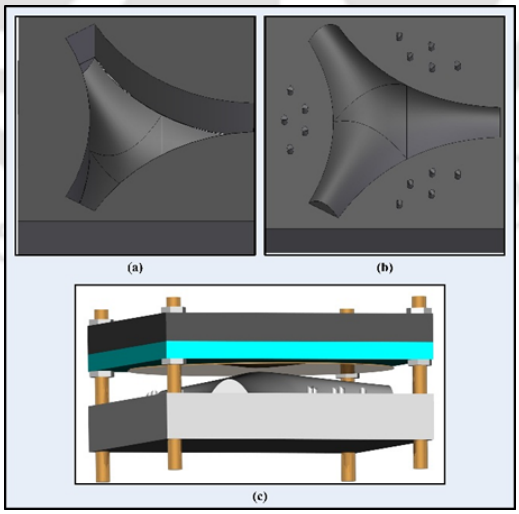

Figure 5.2: EMFP die and setup (a) Negative die (b) Positive die (c) Assembled setup with coil

EMFP with the negative die was not able to fill the cavity due to dead zone at the centre of the coil, therefore a positive die was made to carry out the EMFP

process to overcome the dead zone. The overall size of the die used was 250 mm square with the height of 60 mm. Total 15 number of 6 mm diameter punches were placed around the die. The maximum deformation of the sheet is limited by the height of the die.

From the series of experiments it was found that 5.2 kJ of energy is sufficient to do simultaneous forming and perforation of AA 1050 sheet of thickness 1 mm. EMFP die was manufactured by using sand casting process. The pattern necessary to create the die cavity was manufactured in thermocol material as shown in Figure 5.3. The material used for manufacturing the die was gray cast iron as it has a low electrical conductivity which does not lead to generation of significant eddy currents in the die. It is easy to cast this material and also it has good damping properties.

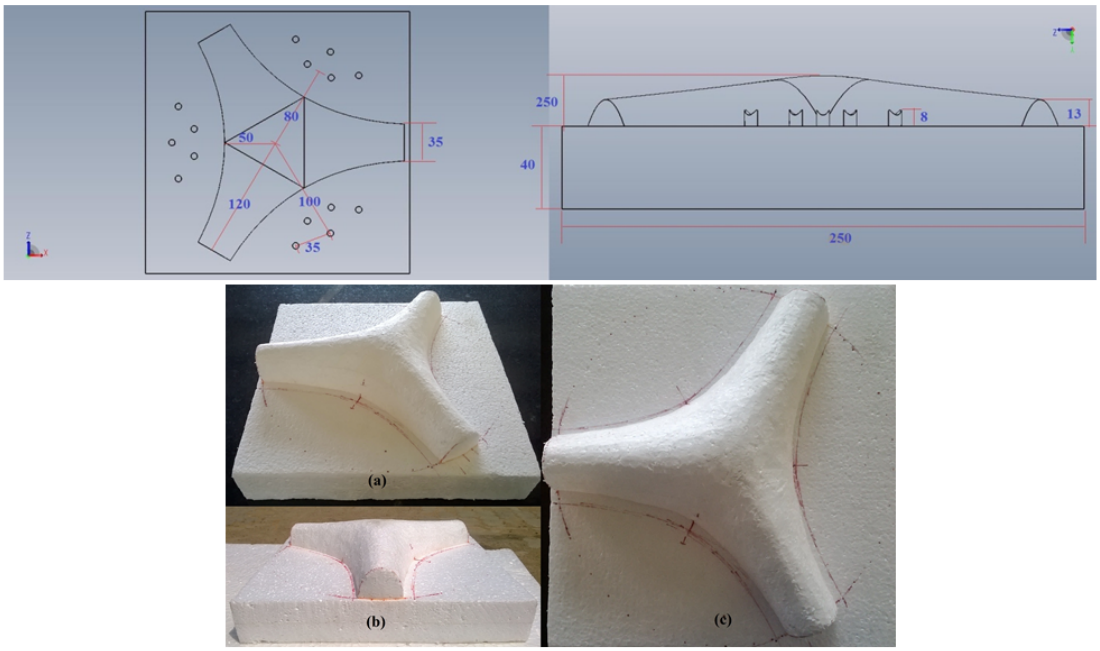

Figure 5.3: Pattern used to create die cavity

The die was then finished with power grinding to give a smooth finish to the die. The finished die is shown in Figure 5.4. The finished die will lead to smooth forming of the sheet and to reduce the friction. Further reduction in the friction can be achieved by getting the mirror finish and lapping of the die. Use of lubricants can also increase the forming limit. An array of holes were created on the flat face of the die for fitting punches necessary for perforation operation.

Figure 5.4: EMFP die

5.2 Punch for EMFP

A punch was designed as an integral part of the die for EMFP operation. Design of punch was very important to get the desired perforation. Two types of punches, namely pointed and concave were used to perform the EMFP operation as shown in Figure 5.5

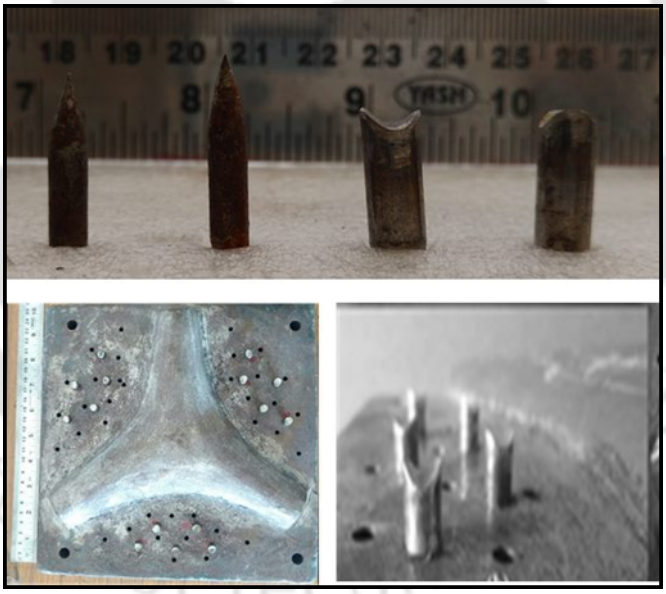

Figure 5.5: EMFP punch and die

5.3 Coil

As the component to be formed has features away from the centre, the electromagnetic forming coil was designed so that most of the energy was concentrated away from the centre. A flat seven turn spiral coil with 15 mm pitch was made from 6 mm diameter copper rod. The pitch in the coil was chosen to avoid sparking between turns. The seven-turn spiral coil was then coated with epoxy resin for

insulation purpose. The coil material used in the experiment was copper (99.99 % pure). The coil has maximum radius 150 mm with pitch 15 mm and 7 turns as shown in Figure 5.6.

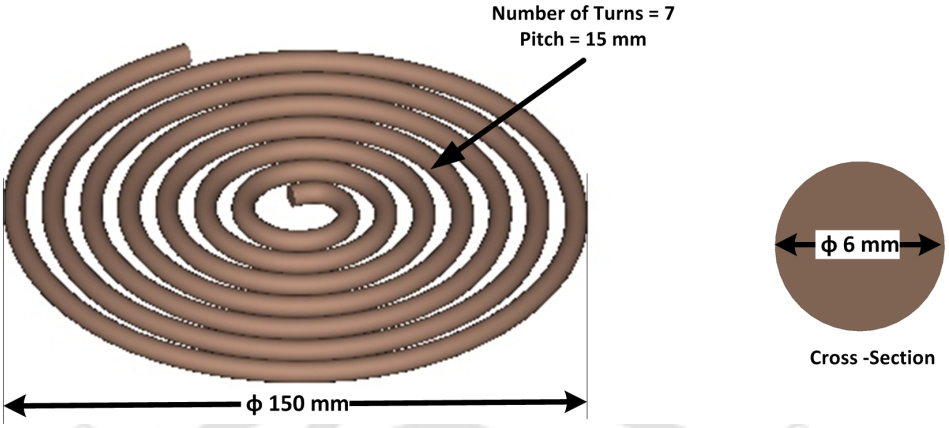

Figure 5.6: EMFP coil dimensions

A photograph of the coil used for experimental work is shown in Figure 5.7 below. It shows the seven turn coil embedded in epoxy resin. Top and bottom sheets of FRP protect the coil from getting in contact with the sheet or other experimental devices. The end lugs were used to connect the coil to high voltage terminals from the capacitor bank.

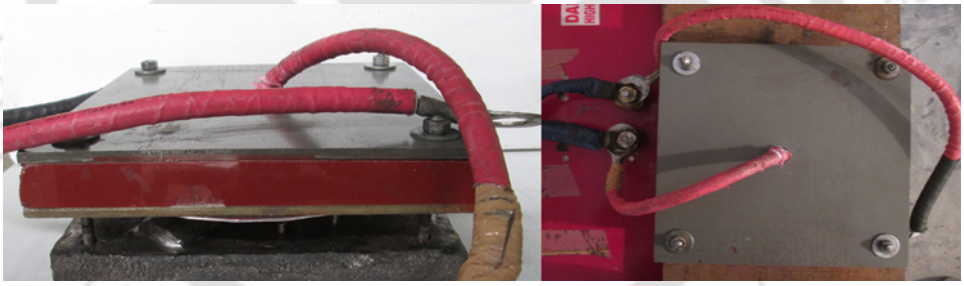

Figure 5.7: EMFP coil

5.4 EMFP Setup

EMFP setup was assembled as shown in Figure 5.8. The die was kept flat on the table and fixed with bolts in the corners. On top of die flat sheet was placed touching to the die directly. The coil insulated with epoxy was kept upside down so that the top face of coil faced towards the bottom. Thus the placed coil was then bolted with the die and the table.

Two types of punches were used, namely pointed and concave, as shown in Figure 5.9 and Figure 5.10 respectively. Pointed punches were not able to remove the blanks, and concave punches were able to remove the blanks.

Figure 5.8: EMFP coil and formed samples

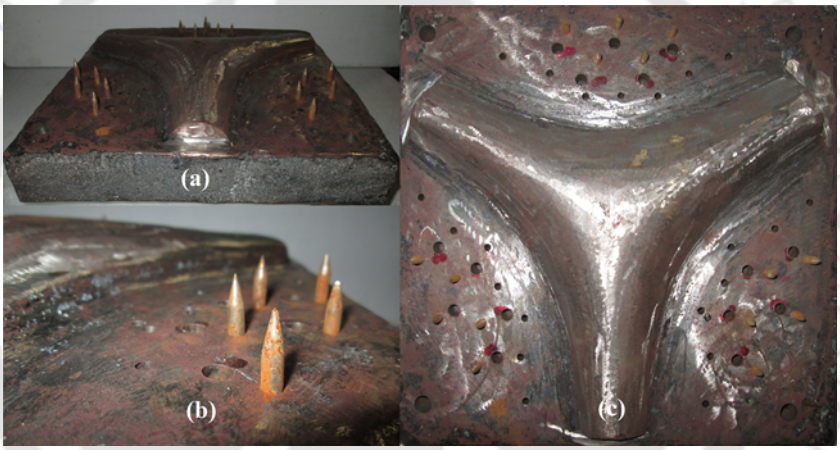

Figure 5.9: EMFP die with pointed punch

5.5 Results and Discussion

Electromagnetic Forming and Perforation (EMFP) was carried out for AA 1050 and AA 5052. To study the effect of process parameters, discharge energy for deformation was varied from 3.1 kJ to 7.5 kJ.

In EMFP operation the desired diameter of the hole was 6 mm which was expected to be equal to the punch diameter. EMFP resulted in variation in actual hole size of the perforated hole due to the combination of both forming and perforation operation. The perforated hole was found to be of elliptical in shape instead of circular. Elongation of the hole (i.e. increase in the difference between major and minor diameters) was observed with increase in energy. This elongation was due to stretching of sheets, so elongation of the holes can be eliminated by reducing the stretching of sheet.

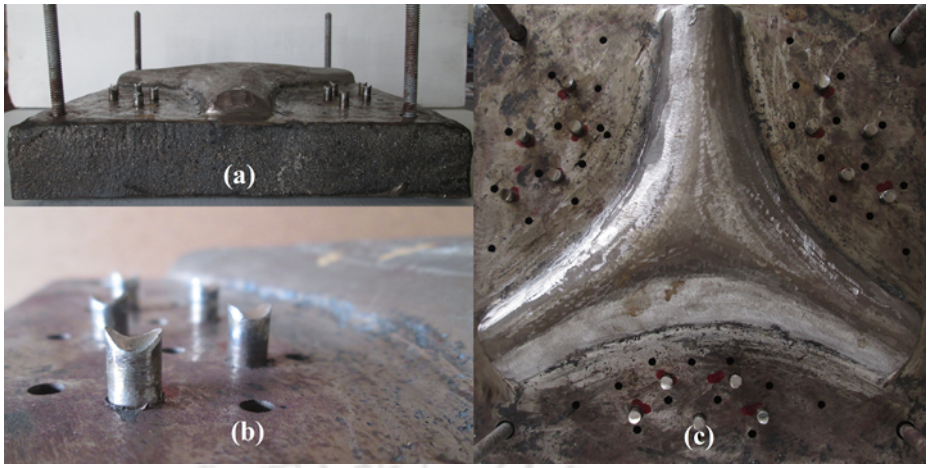

Figure 5.10: EMFP die with concave punch

In order to reduce the stretching of the sheet, discharge energy was decreased. At the same time, perforation of the hole does not take place as the discharge energy was decreased to a large extent. Therefore, an optimum value of discharge energy was found out to perform the EMFP process, which results into successful forming with the minimum elongation of holes punched. The maximum deformation height (H) was measured from the flat face of the sheet to the tip of the dome formed. The difference between the major diameter (D) and the minor diameter (d) of the punched hole gives the measure of the difference in the diameters due to stretching. The major diameter of the hole was measured in the radial direction while the minor diameter was measured along the angular direction. The minor diameter was nearly equal to the actual diameter of the hole while holes get elongated in the radial direction. Figure 5.11 shows the nomenclature of dome height (H), maximum deformation height (h), hole diameter (d), major diameter (D) and minor diameter (d) of elongated elliptical hole.

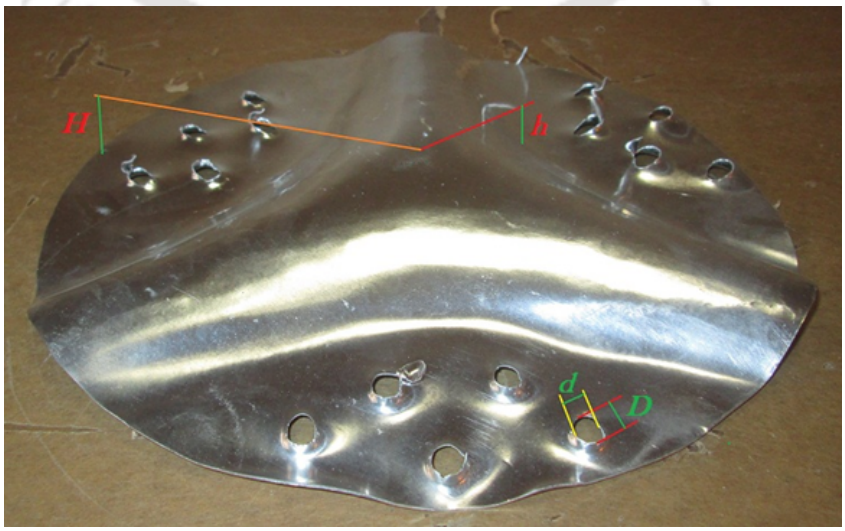

Figure 5.11: Nomenclature for dome height and hole elongation

Firstly, EMFP operations were carried out using pointed punches but they were not able to perforate the holes. Therefore, concave punches were used in place of pointed punches. EMFP was performed for AA1050 using concaved punches as shown in Figure 5.12. During the EMFP of AA 1050, hardness increases with the increase in discharge energy. The AA 1050 sample had an average hardness of 45 HV, after EM forming its hardness was increased by 1.3 times at discharge energy of 5.2 kJ and 1.51 times at discharge energy of 7.5 kJ.

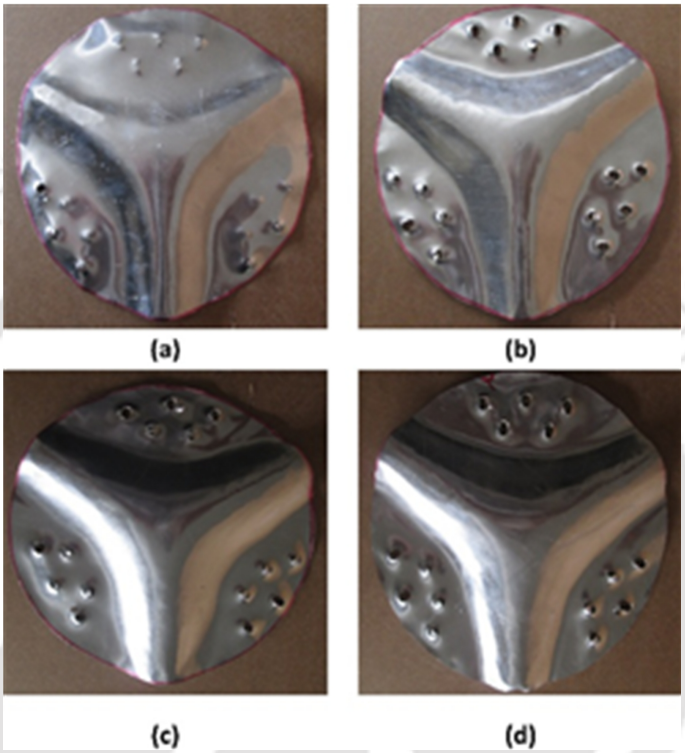

Figure 5.12: EMFP of AA 1050 (a) 3.1 kJ (b) 3.7 kJ (c) 4.4 kJ (d) 5.2 kJ

For AA 1050, the discharge energy of 3.1 kJ was able to perforate only one hole. It was observed that the discharge energy of 3.1 kJ was insufficient to deform the sample and perforate all the holes in the sheet. A further increase in energy to 3.7 kJ increases the number of holes perforated to six. However, the energy was still insufficient to perforate all the holes. A further increase in discharge energy to 4.4 kJ, results into ten perforated holes. Finally, the discharge energy of 5.2 kJ results in to perforation of all 15 holes. Further, increase in energy at 6.0 kJ, 6.8 kJ and 7.3 kJ also results into forming and perforation of the sheet but elongation of the perforated holes increases. Therefore, the minimum energy required to perforate all holes in AA 1050 sheets was 5.2 kJ.

In a similar manner the EMFP process was carried out for AA 5052 material. Figure 5.13 shows the EMFP formed AA 5052 samples. As we have discussed, AA 1050 requires 5.2 kJ of energy to perform a successful EMFP operation but in case of AA 5052, the 5.2 kJ discharge energy was insufficient to perforate all

the holes. AA 5052 requires more energy as compared to AA 1050 to perform the EMFP process, due to higher strength of the AA 5052 material as compared to AA 1050. In case of AA 5052, it was not possible to perforate all the holes due to the limitation of the capacitor bank, and doing experiments with further increase in energy was not possible. The maximum number of holes perforated in case of AA 5052 was 9 at 7.5 kJ of energy.

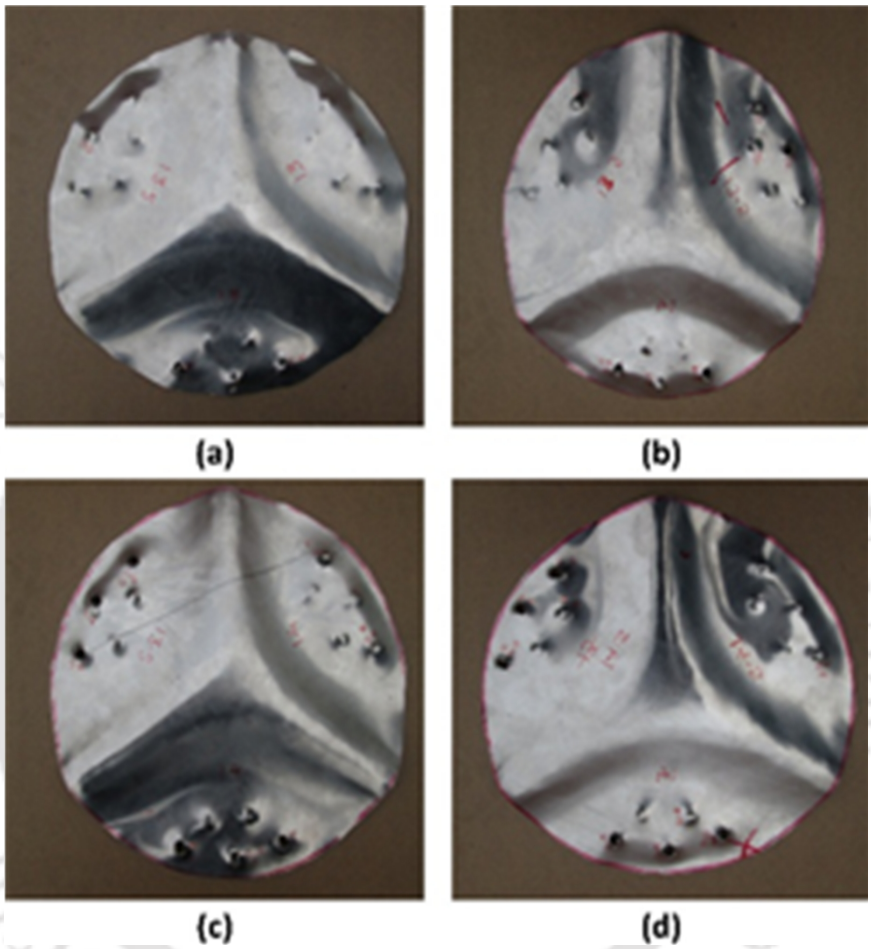

Figure 5.13: EMFP of AA 5052 (a) 5.2 kJ (b) 6 kJ (c) 6.9 kJ (d) 7.5 kJ

Figure 5.14 shows the variation of dome height with respect to discharge energy. Maximum dome height of 21 mm was obtained in case of AA 1050 at discharge energy of 7.5 kJ. Figure 5.15 shows the number of holes perforated with respect to the discharge energy. In case of AA 1050, all 15 holes get perforated at discharge energy of 5.2 kJ. In case of AA 5052, only three holes get perforated at discharge energy of 5.2 kJ. Further increase in energy to 6 kJ and 7.5 kJ resulted in perforation of maximum 7 and 9 number of holes.

The elongation (the difference in major and minor diameter) of the elliptical hole was measured at different values of discharge energies for AA 1050 using concave punches. Figure 5.16 shows variation in elongation of holes with variation in discharge energy. It shows that as the discharge energy was increased, the elongation

of holes also increases. Elongation of holes obtained was found to be less in case of AA 5052 as compared to AA 1050. Table 5.1 and 5.2 summarizes the experimental results of EMFP.

Table 5.1: Effect of discharge energy on dome height

Energy (kJ)	Dome Height (mm)	
	AA 1050	AA 5052
5.2	15.1	11.2
6.0	17.6	11.5
6.8	19.8	12.8
7.5	21	14.3

Table 5.2: Effect of discharge energy on number of holes perforated

Energy (kJ)	Number of Holes Perforated	
	AA 1050	AA 5052
5.2	15	3
6.0	15	7
6.8	15	8
7.5	15	9

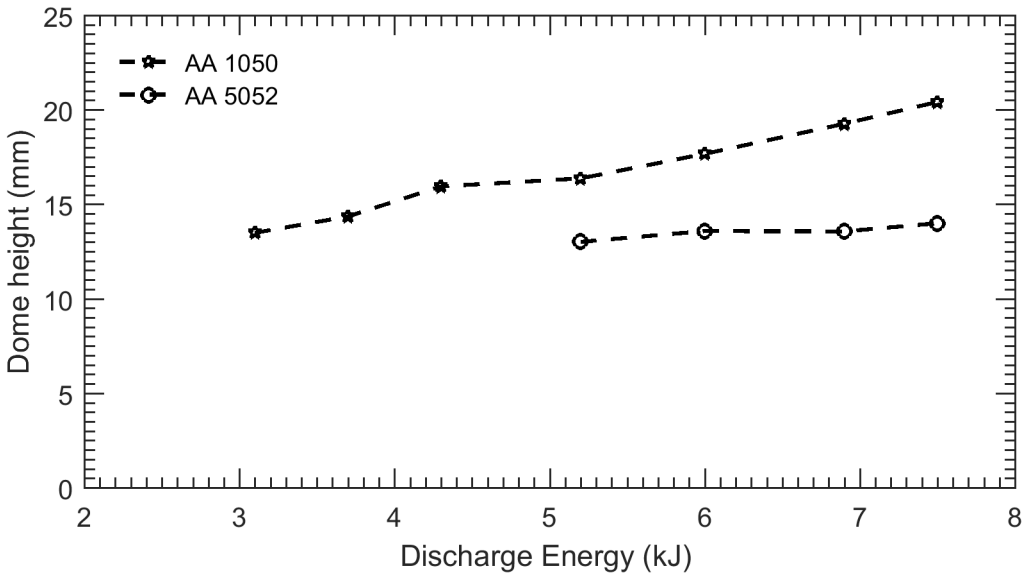

Figure 5.14: Dome height with respect to discharge energy

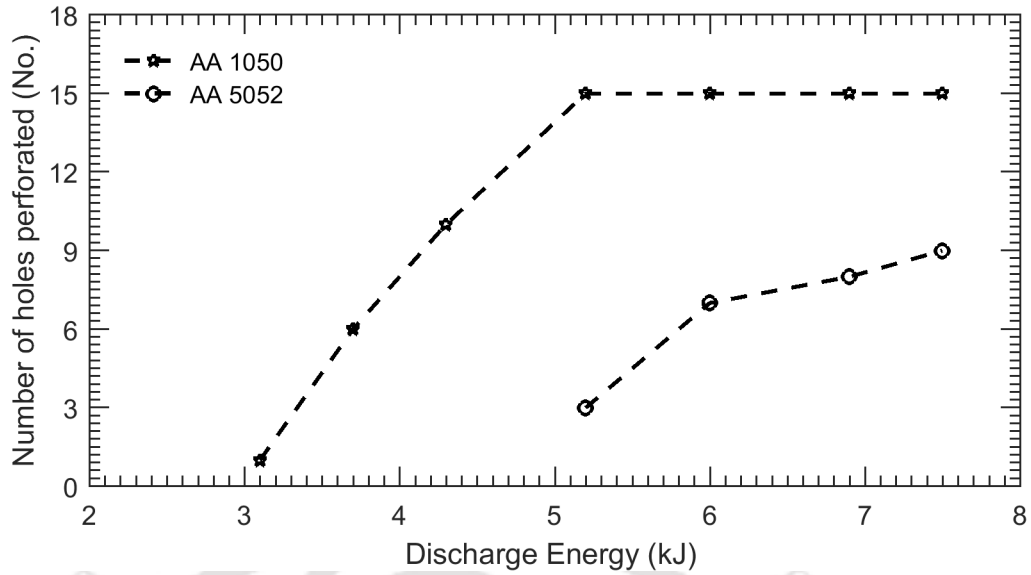

Figure 5.15: Number of holes perforated with respect to discharge energy

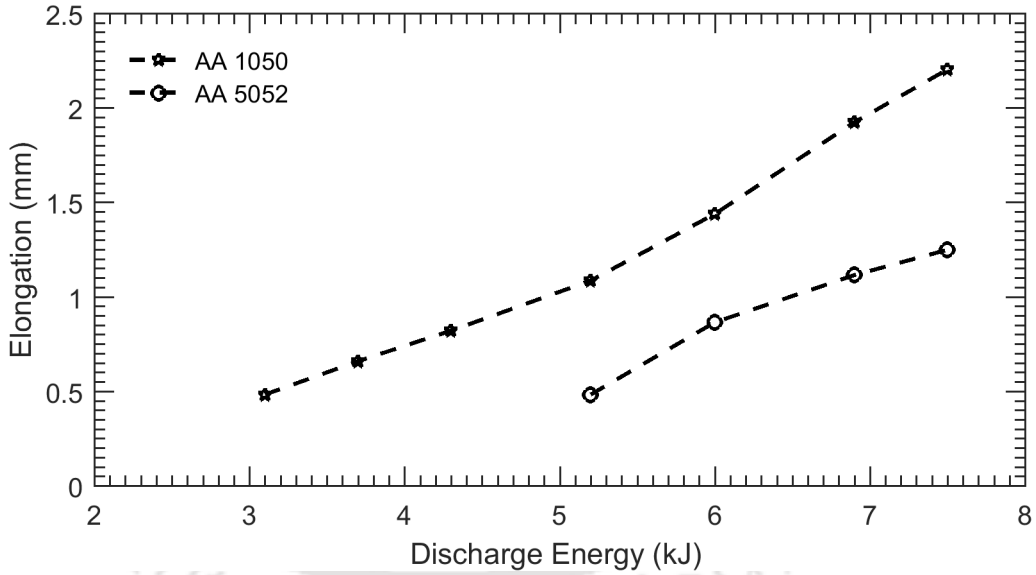

Figure 5.16: Elongation of holes perforated with respect to discharge energy

5.6 FEM Analysis of EMFP

In order to study the electromagnetic forming and perforation, finite element simulations were performed. Initially, we tried to simulate EMFP using the coupled approach. To simulate the EMFP, firstly we simulated the bullet piercing sheet problem and we were successful in simulating it. But when we were applying the same approach to the EMFP, the sheet was distorted into separate pieces. As to refine the simulation results, the mesh size has been decreased but due to

the limitation on the number of nodes further study was not possible. Then, we tried to model the EMFP using ANSYS but due to unavailability of the coupled electromagnetic structural model, we shifted over to the loosely coupled approach to simulate the EMFP process. The finite element analysis of electromagnetic forming and perforation of the sheet was divided into two steps as electromagnetic analysis step and mechanical deformation step. In the present finite element model, the effect of structural deformation on the electromagnetic field has not been taken in to account. The steps to perform finite element analysis of electromagnetic forming and perforation of sheets is shown in Figure 5.17.

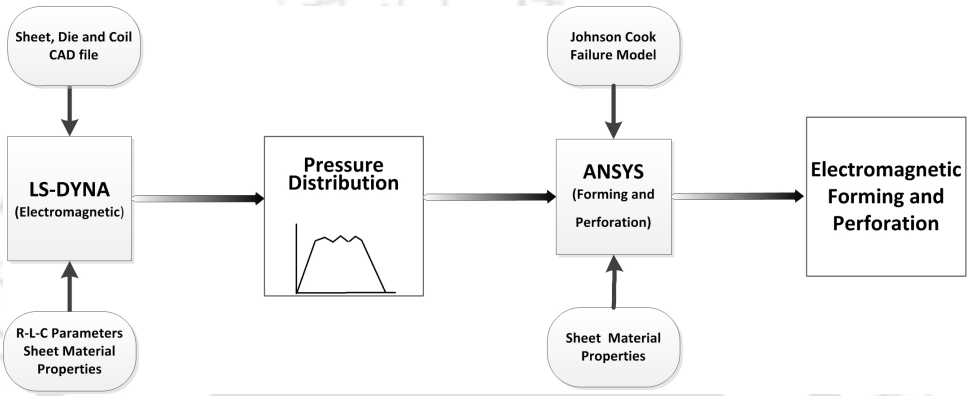

Figure 5.17: Methodology for EMFP simulation

The electromagnetic analysis was performed using LS-DYNA FEM package, to get the pressure distribution on the tube during electromagnetic forming. The pressure distribution obtained from the electromagnetic analysis was used as load for mechanical analysis in ANSYS. A 7-turns copper spiral coil is used with 15 mm pitch. Table 5.3 shows the coil and workpiece material properties used to carry out the simulations. The sheet with thicknesses 1 mm was used and the minimum energy required to perform electromagnetic forming and perforation was studied. The distance between the coil and the sheet is 1.5 mm. The radius of the sheet is 120 mm.

The finite element model created to study the electromagnetic forming and perforation of sheet is shown in Figure 5.18.

Table 5.3: Coil and workpiece parameters used for EMFP simulation

Coil	Number of Turns	7
	Maximum diameter	300 mm
	Circuit inductance	3.1 µH
	Diameter	240 mm
Workpiece	Thickness	1 mm
	Density	2750 kg/m^3
	Young's modulus	80.7 GPa
	Poisson's ratio	0.4
	Conductivity	36 MS/m

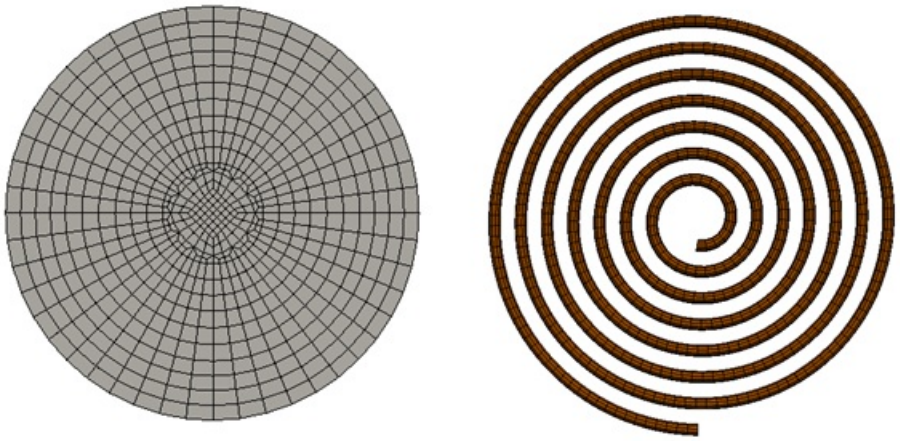

Figure 5.18: Finite element mesh for sheet and coil

The hexahedral solid elements were used to mesh the finite element model. The dimensions of the sheet are 120 mm diameter with 1 mm thickness. The material of the sheet is AA 5052 and AA 1050. The dimensions for the coil are 120 mm diameter, 15 mm pitch and 6 mm cross section of wire. The total elements used for meshing are 2300. The material of the coil is copper. The gap kept between the sheet and the coil is 0.5 mm.

The Johnson-cook material model was used for the workpiece. The Johnson-cook equation is given by [55]

$$\sigma = (A + B\bar{\varepsilon}_p^n)(1 + C \ln \dot{\varepsilon^*}) \tag{5.1}$$

where σ is the equivalent stress; ε_p is the equivalent plastic strain; $\dot{\varepsilon^*}$ is the relative strain rate; A, B, C, and n are J-C material constants. Parameters of Johnson-Cook model for AA 5052 used for simulations are tabulated in Table 5.4.

Table 5.4: AA 1050 material constants for Johnson Cook constitutive model

Poisson's Ratio	0.33	**A** (MPa)	60
Density (kg/m^3)	2680	**B** (MPa)	373.8
Elastic Modulus (GPa)	70	**C**	0.002
Resistivity ($\Omega.m$)	0.049	**n**	0.42
T_m (K)	925	**m**	1.34

To model the perforation, Johnson–Cook damage model was used as given by

$$D = \sum \frac{\triangle \dot{\varepsilon_p}}{\varepsilon_f} \tag{5.2}$$

where $\triangle \varepsilon_p$ is the equivalent plastic strain increment ε_f is the equivalent strain to failure given by the following equation:

$$\varepsilon_f = (d_1 + d_2 \exp -d_3\phi)(1 + d_4 \ln \frac{\dot{\varepsilon_p}}{\varepsilon_n}) \tag{5.3}$$

where D is the J-C damage parameter, which is equal to 0 initially and is equal to 1 during material fracture. As the J-C damage parameter for a material reaches the critical value of 1, the elements get deleted. Surface to surface contact is defined between the die and the workpiece. $\dot{\varepsilon_p}$ is the equivalent plastic strain rate, d_1, d_2, d_3 and d_4 are J-C damage model constants, and ϕ is the stress-triaxiality factor defined as the ratio of averaged normal stress (σ_m) and von-mises equivalent stress (σ). The first bracket expression represents the dependence of the fracture on pressure and explains the decrease in strain to fracture as the hydrostatic stress (σ_m) increases. The second bracket expression represents the effect of strain rate on the strain to fracture. The first bracket expression represents the dependence of the fracture on pressure and explains the decrease in strain to fracture as the hydrostatic stress (σ_m) increases.

5.7 Results of EMFP Simulations

The numerical simulation of electromagnetic forming and perforation is carried out at various energy levels. Figure 5.19 shows the variation of current pulse at various energy levels. The current curve is given as the input to the electromagnetic forming and perforation model.

The magnetic pressure distributions calculated from the simulation are shown in Figure 5.20. The magnitude of both magnetic field and magnetic pressure decreases with time due to damped nature of the current.

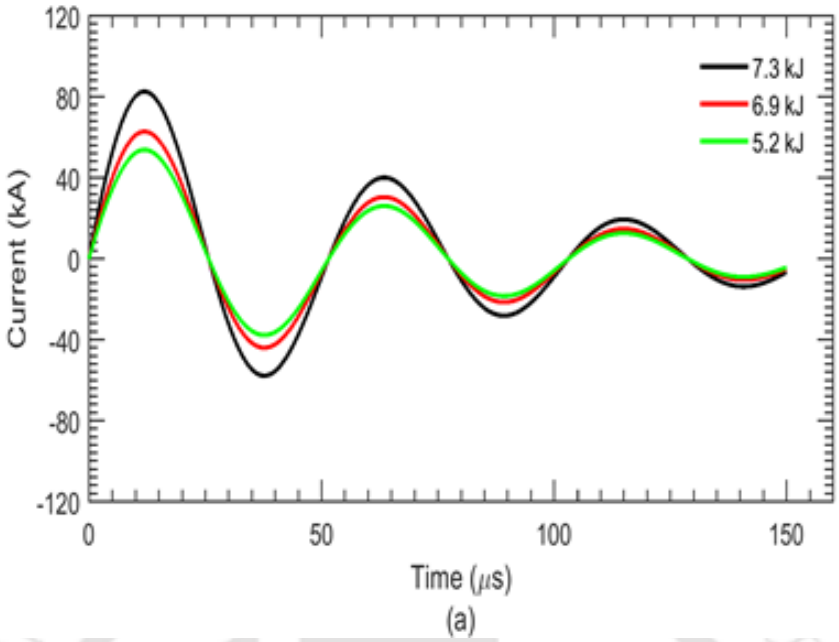

Figure 5.19: Current curve used for EMFP simulation

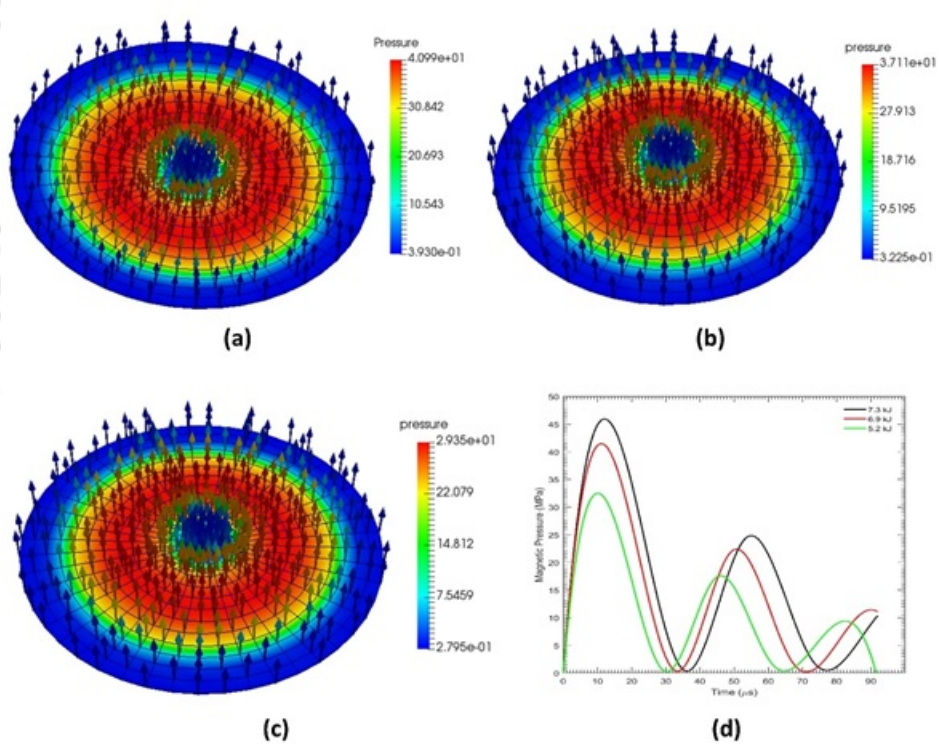

Figure 5.20: Pressure distribution during EMFP

The pressure distribution obtained above is given as input to the forming model. Figure 5.21 shows the simulation result obtained from the forming and perforation model. The pressure distribution given to the forming model corresponds to the percentage of energy discharged from the capacitor bank. It has

been found that, as the discharge energy increases, number of holes perforated will also increase till optimum discharge energy. All 15 holes are completely perforated at the minimum discharge of 5.3 kJ. Hence 5.3 kJ discharge energy can be treated as optimum energy for EMFP. The velocity of impact came out to be 185.06 m/s, which is the minimum velocity required for the sheet to perforate as per the die shape.

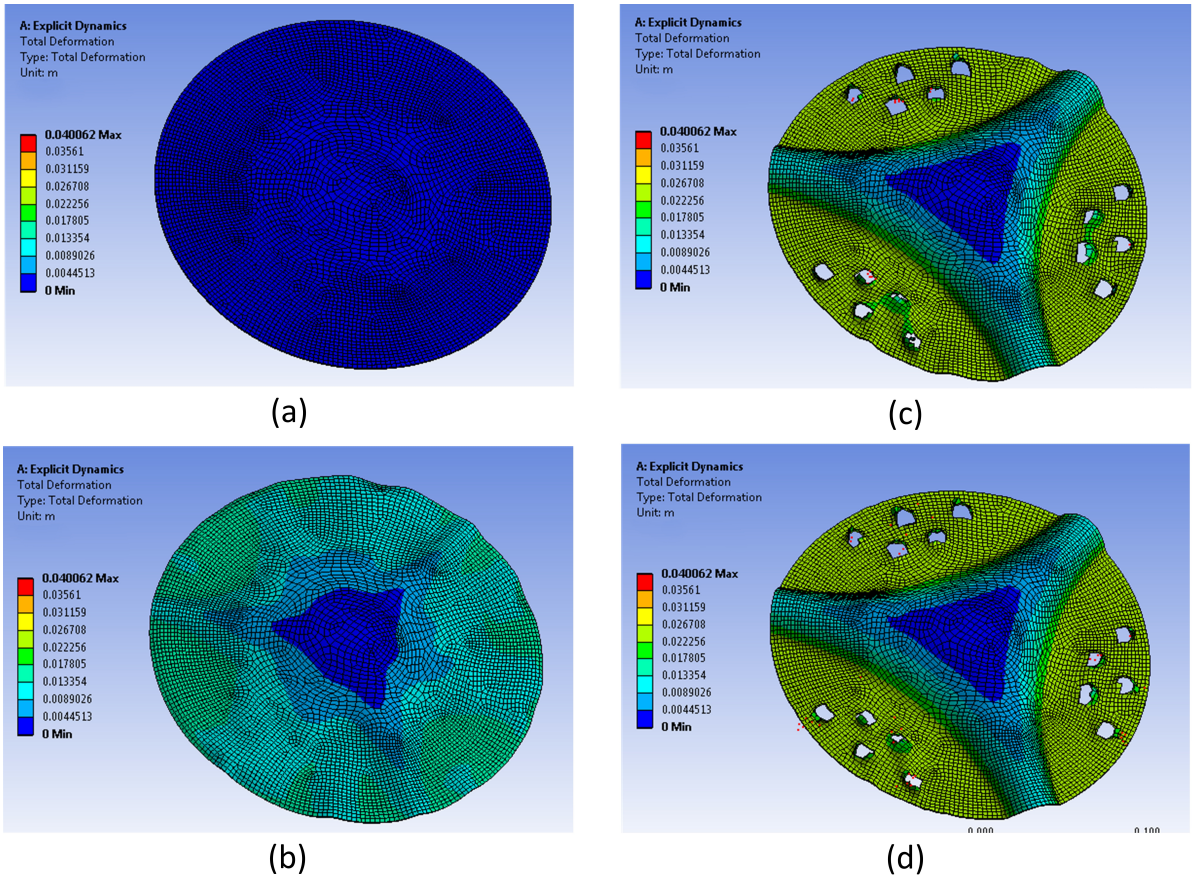

Figure 5.21: Deformation and perforation of sheet with time (a) 0 s (b) 75 s (c) 180 s (d) 210 s

Assuming the sheet comes to rest after perforation, the minimum velocity required to perforate the holes is given by

$$\text{Rate of change of Momentum} = \text{Net Force}$$

$$\begin{aligned} mV_{min} &= k(n\pi dt\tau T) \\ \rho\frac{\pi D^2 t}{4}V_{min} &= k(n\pi dt\tau T) \\ V_{min} &= \frac{dn\tau}{100D^2\rho} \end{aligned} \tag{5.4}$$

where n is the number of holes perforated, d is the punch diameter, k is constant to account for deformation, T is the time, τ is the shear strength, D is the sheet diameter and ρ is the density. Figure 5.22 shows the minimum velocity required to perforate a particular number of holes. It shows that the minimum velocity required to perforate holes increases as the number of holes to perforate increases.

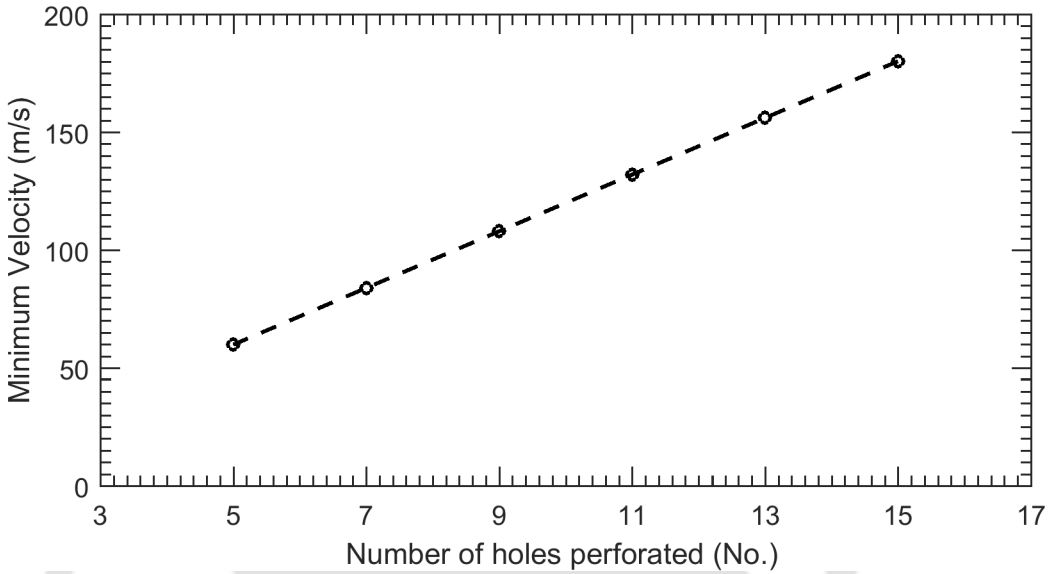

Figure 5.22: Minimum velocity required to perforate the sheet

5.8 Summary

1. The concaved punch gives better perforation as compared to the pointed punch.

2. The extent of elongation increases with the increase in punch length, dome height and discharge energy.

3. For AA 1050 the optimum value of discharge energy is 5.2 kJ in the concaved punch case. At this discharge energy, the dome height is 19.7 mm and the extent of elongation is 2 mm.

4. For AA 5052 the optimum value of discharge energy is more than 7.3 kJ (around $7.5 - 7.8$ kJ) in the concaved punch case. At the discharge energy of 7.3 kJ, the dome height is 14.33 mm and the extent of elongation is 1.16 mm.

5. For AA 1050, its hardness increased 1.3 times the original hardness at the discharge energy of 5.2 kJ and 1.51 times at the discharge energy of 7.5 kJ.

In AA 5052, hardness increased to 1.17 times at the discharge energy of 7.3 kJ.

6. The electromagnetic forming and perforation process is simulated using FEM in a sequentially coupled way. Firstly the electromagnetic pressure is computed which acts as an input to the forming and perforation model. Secondly, the magnetic pressure obtained from the electromagnetic model is given as the input to the forming and perforation model to calculate the stress, strain distribution and velocity of the sheet.

CHAPTER 6

Conclusions and Scope of Future Work

6.1 Conclusions

1. The electromagnetic tube experiments are performed to determine the effect of coil-tube relative length during forming. Finite element simulations are validated with the experiment to know the effect of parameters during electromagnetic tube expansion.

2. For coil-tube relative length smaller than one, non-uniform deformation of the tube takes place with maximum deformation at the centre of the tube. For coil-tube relative length equal to one, uniform deformation of the tube takes place. For coil-tube relative length greater than one, non-uniform deformation of tube takes place with maximum deformation at tube ends.

3. Magnetic pressure available for deformation decreases with the increase in coil length during electromagnetic tube expansion.

4. The validated finite element simulations are used to study the effect of frequency during electromagnetic tube expansion. The simulation result shows that initially, the deformation of the tube increases with frequency due to the decrease in skin depth as the frequency increases. As the frequency is increased beyond the optimum value, deformation of the tube start decreasing due to the out of phase of eddy current.

5. The effect of frequency during electromagnetic tube expansion is more prominent for the thin tube as compared to thick tubes.

6. The contribution of the current pulse during electromagnetic sheet forming is studied by crow-barring the current pulse. The results show that only 1.5 cycles of the current pulse are responsible for the deformation of the sheet.

7. Dual electromagnetic sheet forming using uniform pressure actuator has been carried out to eliminate the effect of the bottom layer of the coil.

8. Electromagnetic sheet forming and perforation has been carried out using two types of punches, viz pointed and concaved. The concaved punches were found to give better perforation as compared to the pointed punches.

9. During electromagnetic forming and perforation of a sheet, perforated holes get elongated in the radial direction due to simultaneous forming and perforation of the sheet. The elongation of holes increases with the increase in discharge energy. At the same time, lower discharge energy leads to improper perforation and forming. For AA 1050 sheet, the optimum value of discharge energy to perform electromagnetic forming and perforation is found to be 5.2 kJ.

6.2 Scope of Future Work

1. As the experimental results were well correlated with the simulation results, simulations can be used to obtain the optimum parameters required to design a machine for a particular application.

2. As the flat spiral coil leads to the non-uniform distribution of magnetic field, a flat spiral coil can be designed with varying cross-section to study the effect of the electromagnetic field distribution.

3. To perform the crow-barring of the current pulse during electromagnetic forming, the crow-barring circuit can be designed to increase the efficiency of the machine and life of the coil.

4. Deformation of low conductive metals can be studied using a driver plate and optimum thickness of the driver plate can be obtained to perform the electromagnetic forming.

5. Another possible idea is performing electromagnetic forming and perforation of the sheet with more number of holes and further optimization of punch shapes to obtain improved shear edges. High speed video of the sheet can be recorded as it comes in contact with the punch and die to analyze the impact conditions and shearing during the process.

REFERENCES

[1] S. Hecker, Formability of aluminum alloy sheets, Journal of Engineering Materials and Technology 97 (1) (1975) 66–73.

[2] Z. Tekıner, An experimental study on the examination of springback of sheet metals with several thicknesses and properties in bending dies, Journal of Materials Processing Technology 145 (1) (2004) 109–117.

[3] D. J. Mynors, B. Zhang, Applications and capabilities of explosive forming, Journal of Materials Processing Technology 125 (2002) 1–25.

[4] C. Maris, A. Hassannejadasl, D. E. Green, J. Cheng, S. F. Golovashchenko, A. J. Gillard, Y. Liang, Comparison of quasi-static and electrohydraulic free forming limits for DP 600 and AA 5182 sheets, Journal of Materials Processing Technology 235 (2016) 206–219.

[5] J. T. Conway, Exact solutions for the magnetic fields of axisymmetric solenoids and current distributions, IEEE Transactions on Magnetics 37 (4) (2001) 2977–2988.

[6] F. W. Grover, Inductance calculations: working formulas and tables, Courier Corporation, 2004.

[7] I. Ulacia, I. Hurtado, J. Imbert, C. Salisbury, M. Worswick, A. Arroyo, Experimental and numerical study of electromagnetic forming of AZ 31B magnesium alloy sheet, Steel Research International 80 (5) (2009) 344–350.

[8] G. Mamalis, D. Manolakos, A. Kladas, A. Koumoutsos, S. Ovchinnikov, Electromagnetic forming of aluminum alloy sheet using a grooved die: numerical modeling, The Physics of Metals and Metallography 102 (1) (2006) 90–93.

[9] K. Faes, O. Zaitov, W. De Waele, Electromagnetic pulse crimping of axial form fit joints, in: Proceedings of the 4th International Conference on High Speed Forming, 2012, pp. 229–242.

[10] H. Yu, Z. Xu, Z. Fan, Z. Zhao, C. Li, Mechanical property and microstructure of aluminum alloy-steel tubes joint by magnetic pulse welding, Materials Science and Engineering: A 561 (2013) 259–265.

[11] X. Cui, J. Mo, S. Xiao, E. Du, J. Zhao, Numerical simulation of electromagnetic sheet bulging based on FEM, The International Journal of Advanced Manufacturing Technology 57 (1-4) (2011) 127–134.

[12] J. R. Johnson, G. Taber, A. Vivek, Y. Zhang, S. Golowin, K. Banik, G. K. Fenton, G. S. Daehn, Coupling experiment and simulation in electromagnetic forming using photon doppler velocimetry, Steel Research International 80 (5) (2009) 359–365.

[13] P. Vanhulsel, M. Van Wonterghem, W. De Waele, K. Faes, Groove design for form fit joints made by electromagnetic pulse crimping, in: Sustainable Construction and Design, Vol. 2, 2011, pp. 432–441.

[14] K. Faes, O. Zaitov, W. De Waele, Electromagnetic pulse crimping of axial form fit joints, in: Proceedings of the 5th International Conference on High Speed Forming, 2012, pp. 229–242.

[15] V. Psyk, D. Risch, B. Kinsey, A. Tekkaya, M. Kleiner, Electromagnetic forming—a review, Journal of Materials Processing Technology 211 (5) (2011) 787–829.

[16] A. Mamalis, D. Manolakos, A. Kladas, A. Koumoutsos, Electromagnetic forming and powder processing: Trends and developments, Applied Mechanics Reviews 57 (4) (2004) 299–324.

[17] P. Kapitza, A method of producing strong magnetic fields, Proceedings of the Royal Society of London 105 (734) (1924) 691–710.

[18] G. Harvey, D. Brower, Metal forming device and method, US Patent 2,976,907 (Mar. 28 1961).

[19] W. Xu, H. Fang, W. Xu, Analysis of the variation regularity of the parameters of the discharge circuit with the distance between workpiece and inductor for electromagnetic forming processes, Journal of Materials Processing Technology 203 (1) (2008) 216–220.

[20] V. Psyk, C. Beerwald, A. Klaus, M. Kleiner, Characterisation of extruded magnesium profiles for electromagnetic joining, Journal of Materials Processing Technology 177 (1) (2006) 266–269.

[21] G. S. Daehn, High-velocity metal forming., Metalworking: Sheet Forming(ASM Handbook Volume 14 B) 14 (2006) 405–418.

[22] J. Bednarczyk, Distributions of forces in the inductors used in metal processing in the pulse magnetic field, Journal of Materials Processing Technology 133 (3) (2003) 340–347.

[23] T. Baaten, N. Debroux, W. De Waele, K. Faes, Joining of copper to brass using magnetic pulse welding, in: Proceeding of the 4th International Conference on High Speed Forming, 2010, pp. 84–96.

[24] M. Kamal, G. S. Daehn, A uniform pressure electromagnetic actuator for forming flat sheets, Journal of Manufacturing Science and Engineering 129 (2) (2007) 369–379.

[25] S. Golowin, M. Kamal, J. Shang, J. Portier, A. Din, G. S. Daehn, J. R. Bradley, K. E. Newman, S. Hatkevich, Application of a uniform pressure actuator for electromagnetic processing of sheet metal, Journal of Materials Engineering and Performance 16 (4) (2007) 455–460.

[26] H. Yu, C. Li, Z. Zhao, Z. Li, Effect of field shaper on magnetic pressure in electromagnetic forming, Journal of Materials Processing Technology 168 (2) (2005) 245–249.

[27] M. A. Bahmani, K. Niayesh, A. Karimi, 3D simulation of magnetic field distribution in electromagnetic forming systems with field-shaper, Journal of Materials Processing Technology 209 (5) (2009) 2295–2301.

[28] S. F. Golovashchenko, Material formability and coil design in electromagnetic forming, Journal of Materials Engineering and Performance 16 (3) (2007) 314–320.

[29] V. Psyk, C. Beerwald, A. Klaus, M. Kleiner, Characterisation of extruded magnesium profiles for electromagnetic joining, Journal of Materials Processing Technology 177 (1) (2006) 266–269.

[30] M. Kleiner, C. Beerwald, W. Homberg, Analysis of process parameters and forming mechanisms within the electromagnetic forming process, CIRP Annals-Manufacturing Technology 54 (1) (2005) 225–228.

[31] A. Meriched, M. Féliachi, H. Mohellebi, Electromagnetic forming of thin metal sheets, IEEE Transactions on Magnetics 36 (4) (2000) 1808–1811.

[32] F. Song, X. Zhang, Z. Wang, L. Yu, A study of tube electromagnetic forming, Journal of Materials Processing Technology 151 (1) (2004) 372–375.

[33] H. Zhang, M. Murata, H. Suzuki, Effects of various working conditions on tube bulging by electromagnetic forming, Journal of Materials Processing Technology 48 (1-4) (1995) 113–121.

[34] H. P. Yu, C. F. Li, Effects of coil length on tube compression in electromagnetic forming, Transactions of Nonferrous Metals Society of China 17 (6) (2007) 1270–1275.

[35] M. Padmanabhan, Wrinkling and springback in electromagnetic sheet metal forming and electromagnetic ring compression, Ph.D. thesis, The Ohio State University (1997).

[36] S. Al Hassani, J. Duncan, W. Johnson, Techniques for designing electromagnetic forming coils, in: Proceedings of the 2nd International Conference on High Rate Forming, 1969, pp. 5–1.

[37] N. Takatsu, K. Masana, T. Toshimi, High-speed forming of metal sheets by electromagnetic force, JSME International Journal Series A 31 (1) (1988) 142–148.

[38] J. Imbert, S. Winkler, M. Worswick, D. Oliveira, S. Golovashchenko, The effect of tool–sheet interaction on damage evolution in electromagnetic forming of aluminum alloy sheet, Journal of Engineering Materials and Technology 127 (1) (2005) 145–153.

[39] D. Risch, A. Brosius, M. Kleiner, Influence of the workpiece stiffness on the electromagnetic sheet metal forming process into dies, Journal of Materials Engineering and Performance 16 (3) (2007) 327–330.

[40] D. Risch, C. Beerwald, A. Brosius, M. Kleiner, On the significance of the die design for electromagnetic sheet metal forming, in: Proceedings of the Ist International Conference on High Speed Forming, 2004, pp. 191–200.

[41] Q. Cao, X. Han, Z. Lai, Q. Xiong, X. Zhang, Q. Chen, H. Xiao, L. Li, Analysis and reduction of coil temperature rise in electromagnetic forming, Journal of Materials Processing Technology 225 (2015) 185–194.

[42] Q. Xiong, Q. Cao, X. Han, Z. Lai, F. Deng, B. Zhang, X. Zhang, Q. Chen, L. Li, Axially movable electromagnetic forming system for large-scale metallic sheet, IEEE Transactions on Applied Superconductivity 26 (4) (2016) 1–4.

[43] W. Hartmann, M. Romheld, A. Donner, A 100 kJ pulse unit for electromagnetic forming of large area sheet metals, in: Proc. IEEE Power Modulator Symp., 2006, pp. 577–581.

[44] M. Seth, V. J. Vohnout, G. S. Daehn, Formability of steel sheet in high velocity impact, Journal of Materials Processing Technology 168 (3) (2005) 390–400.

[45] D. Oliveira, M. Worswick, M. Finn, D. Newman, Electromagnetic forming of aluminum alloy sheet: free-form and cavity fill experiments and model, Journal of Materials Processing Technology 170 (1) (2005) 350–362.

[46] J. Imbert, M. Worswick, S. Winkler, S. Golovashchenko, V. Dmitriev, Analysis of the increased formability of aluminum alloy sheet formed using electromagnetic forming, Tech. rep., SAE Technical Paper (2005).

[47] G. Lal, M. Hillier, The electrodynamics of electromagnetic forming, International Journal of Mechanical Sciences 10 (6) (1968) 491–500.

[48] Y. Kiliclar, O. Demir, M. Engelhardt, M. Rozgić, I. Vladimirov, S. Wulfinghoff, C. Weddeling, S. Gies, C. Klose, S. Reese, et al., Experimental and numerical investigation of increased formability in combined quasi-static and high-speed forming processes, Journal of Materials Processing Technology 237 (2016) 254–269.

[49] M. Kamal, J. Shang, V. Cheng, S. Hatkevich, G. Daehn, Agile manufacturing of a micro-embossed case by a two-step electromagnetic forming process, Journal of Materials Processing Technology 190 (1) (2007) 41–50.

[50] T. Yamada, K. Kani, K. Sakuma, A. Yubisui, Experimental study on the mechanics of springback in high speed sheet metal forming, in: Proceedings of the 7th International Conference on High Energy Rate Fabrication, 1981, pp. 306–314.

[51] S. Golowin, M. Kamal, J. Shang, J. Portier, A. Din, G. S. Daehn, J. R. Bradley, K. E. Newman, S. Hatkevich, Application of a uniform pressure actuator for electromagnetic processing of sheet metal, Journal of Materials Engineering and Performance 16 (4) (2007) 455–460.

[52] Y. Huang, X. Han, Q. Cao, X. Li, Z. Lai, Y. Lv, L. Li, Design and experimental validation of a pulsed electromagnetic sheet shearing system, IEEE Transactions on Applied Superconductivity 26 (4) (2016) 1–5.

[53] NSF-ATE, Phase lag, Retrieved from, https://www.nde-ed.org/EducationResources/CommunityCollege/EddyCurrents/Physics/phaselag.htm.

[54] Q. Cao, X. Han, Z. Lai, Q. Xiong, X. Zhang, Q. Chen, H. Xiao, L. Li, Analysis and reduction of coil temperature rise in electromagnetic forming, Journal of Materials Processing Technology 225 (Supplement C) (2015) 185 – 194.

[55] A.-C. Jeanson, F. Bay, N. Jacques, G. Avrillaud, M. Arrigoni, G. Mazars, A coupled experimental/numerical approach for the characterization of material behaviour at high strain-rate using electromagnetic tube expansion testing, International Journal of Impact Engineering 98 (Supplement C) (2016) 75 – 87.

List of Publications

1. Patel, C., Ghatule, P. and Kore, S.D., 2017. Finite element analysis of effect of process parameters on electromagnetic free expansion of aluminium tube. *International Journal of Materials and Product Technology*, 54(1-3), pp.165-178.

2. Patel, C. and Kore, S.D., 2017. Finite Element Analysis of Crow-barring Effect During Electromagnetic Forming. *International Journal of Manufacturing Technology and Management*, In press.

3. Patel, C. and Kore, S.D., 2015. Effect of frequency on electromagnetic expansion of thin tubes. *Journal of Machining and Forming Technologies*, 7(1-2), pp.91.

4. Patel, C. and Kore, S.D., 2014. Dual electromagnetic forming using single uniform pressure coil. *Key Engineering Materials*, 611, pp.723-730.